NAVAL POSTGRADUATE SCHOOL

MONTEREY, CALIFORNIA

THESIS

RADAR IMAGING FOR MOVING TARGETS

by

Teo Beng Koon William

June 2009

Thesis Advisor:	Brett H. Borden
Second Reader:	Donald L. Walters

Approved for public release; distribution is unlimited

THIS PAGE INTENTIONALLY LEFT BLANK

REPORT DOCUMENTATION PAGE			*Form Approved OMB No. 0704-0188*
Public reporting burden for this collection of information is estimated to average 1 hour per response, including the time for reviewing instruction, searching existing data sources, gathering and maintaining the data needed, and completing and reviewing the collection of information. Send comments regarding this burden estimate or any other aspect of this collection of information, including suggestions for reducing this burden, to Washington headquarters Services, Directorate for Information Operations and Reports, 1215 Jefferson Davis Highway, Suite 1204, Arlington, VA 22202-4302, and to the Office of Management and Budget, Paperwork Reduction Project (0704-0188) Washington DC 20503.			
1. AGENCY USE ONLY ***(Leave blank)***	**2. REPORT DATE** June 2009	**3. REPORT TYPE AND DATES COVERED** Master's Thesis	
4. TITLE AND SUBTITLE Radar Imaging for Moving Targets		**5. FUNDING NUMBERS**	
6. AUTHOR(S) Teo Beng Koon William			
7. PERFORMING ORGANIZATION NAME(S) AND ADDRESS(ES) Naval Postgraduate School Monterey, CA 93943-5000		**8. PERFORMING ORGANIZATION REPORT NUMBER**	
9. SPONSORING /MONITORING AGENCY NAME(S) AND ADDRESS(ES) N/A		**10. SPONSORING/MONITORING AGENCY REPORT NUMBER**	
11. SUPPLEMENTARY NOTES The views expressed in this thesis are those of the author and do not reflect the official policy or position of the Department of Defense or the U.S. Government.			
12a. DISTRIBUTION / AVAILABILITY STATEMENT Approved for public release; distribution is unlimited		**12b. DISTRIBUTION CODE**	

13. ABSTRACT (maximum 200 words)

Interest in radar imaging has been growing for the past decades because of its long range sensing capabilities. It's continued utility and applications in wide-ranging areas is fundamentally dependant on the ability to produce high-quality, artifact-free imagery. The use of radar to identify and image moving targets remains of great interest for both commercial and military usage. However, when imaging moving targets, there will be issues of incorrect positioning or streaking as the unknown target velocity gives rise to image artifacts. Many techniques have been developed to handle moving objects, however, these techniques make use of the so-called *start-stop* approximation in which target motion is assumed to be momentarily stationary, while it is being interrogated by a radar pulse.

A new linearized imaging theory that combines spatial, temporal and spectral aspects of scattered waves has been developed. This thesis considers the performance of these techniques and compared to existing imaging schemes. It is shown that the new imaging scheme provides better localization and is translation invariant in phase-space. It is also shown that the imaging scheme is dependent on the aperture geometry.

14. SUBJECT TERMS Radar Imaging, Moving Targets, Point Spread Function, Ambiguity Function			**15. NUMBER OF PAGES** 91
			16. PRICE CODE
17. SECURITY CLASSIFICATION OF REPORT Unclassified	**18. SECURITY CLASSIFICATION OF THIS PAGE** Unclassified	**19. SECURITY CLASSIFICATION OF ABSTRACT** Unclassified	**20. LIMITATION OF ABSTRACT** UU

NSN 7540-01-280-5500 Standard Form 298 (Rev. 2-89)
Prescribed by ANSI Std. 239-18

THIS PAGE INTENTIONALLY LEFT BLANK

Approved for public release; distribution is unlimited

RADAR IMAGING OF MOVING TARGETS

Teo Beng Koon William
Major, Republic of Singapore Army
Bachelor of Engineering (Mechanical and Production Engineering), Nanyang Technological University of Singapore, 2003

Submitted in partial fulfillment of the
requirements for the degree of

MASTER OF SCIENCE IN APPLIED PHYSICS

from the

NAVAL POSTGRADUATE SCHOOL
June 2009

Author: Teo Beng Koon William

Approved by: Brett Borden
Thesis Advisor

Donald Walters
Second Reader

James H. Luscombe
Chairman, Department of Physics

THIS PAGE INTENTIONALLY LEFT BLANK

ABSTRACT

Interest in radar imaging has been growing for the past decades because of its long-range sensing capabilities. Its continued utility and applications in wide-ranging areas is fundamentally dependant on the ability to produce high-quality, artifact-free imagery. The use of radar to identify and image moving targets remains of great interest for both commercial and military usage. However, when imaging moving targets, there will be issues of incorrect positioning or streaking, as the unknown target velocity gives rise to image artifacts. Many techniques have been developed to handle moving objects; however, these techniques make use of the so-called *start-stop* approximation in which target motion is assumed to be momentarily stationary while it is being interrogated by a radar pulse.

A new linearized imaging theory that combines spatial, temporal and spectral aspects of scattered waves has been developed. This thesis considers the performance of these techniques compared to existing imaging schemes. It is shown that the new imaging scheme provides better localization, and is translation invariant in phase-space. It is also shown that the imaging scheme is dependent on the aperture geometry.

THIS PAGE INTENTIONALLY LEFT BLANK

TABLE OF CONTENTS

LIST OF FIGURES

THIS PAGE INTENTIONALLY LEFT BLANK

ACKNOWLEDGMENTS

The author is thankful to his thesis advisor, Professor Brett Borden, for his guidance and patience throughout the whole stay at the Naval Postgraduate School. His ability to explain complex concept clearly has indeed made his lesson most insightful and enjoyable. As an advisor, he is constantly supportive and encouraging throughout the thesis work. The author would also like to thank his co advisor, Professor Donald Walters, whose meticulous reading and many insightful comments have contributed a great deal to the flow and clarity of this thesis. Finally, I thank my wife Heather and my son Josiah, who have constantly provided joy and strength throughout this endeavor.

THIS PAGE INTENTIONALLY LEFT BLANK

I. INTRODUCTION

A. RADAR IMAGING HISTORY

Radar imaging is a technology that has been developed mainly within the engineering community. Radar is a sensor system that is widely used to detect, locate and identify targets at great distances in all kinds of weather. Radar's ability to perform such functions unlike many optical sensor systems has made it a proven and well-recognized system for the past 70 years. The fundamental reason for radar's usefulness is its ability to interpret and extract information from the echo signals, and the fact that wavelengths of radar signals makes them relatively unaffected by atmospheric and weather-induced attenuation. However, this behavior causes problems when using radar for imaging: Image resolution depends on signal wavelength. Radar systems generally use longer wavelengths and hence suffer reduced image resolution compared with other systems. Nevertheless, radar is still sensitive to objects whose length scales range from centimeters to meters. This is because radar waves scatter from objects whose size is on the same order as the transmitted signal wavelength or larger, and many objects of interest are in this range.

Radar programs started in the 1930s and much research and development work has been done to improve the use of radar for imaging. Many radar imaging techniques have also been developed to increase the resolution of radar-based imaging. Examples of the key inventions are the Synthetic-Aperture Radar (SAR) and Inverse Synthetic-Aperture Radar (ISAR), which were developed due to interest in operational concepts. The key goal in both of these applications is the ability to produce high-quality, artifact-free imagery.

B. IMAGING TECHNIQUES TO CREATE ARTIFACT-FREE IMAGERY

Radar-based imaging techniques have evolved considerably over many decades. One common objective among these developments is to obtain an artifact-free image. Many implicit assumptions are embedded in these techniques, which are discussed in

many journal papers. Among these assumptions, the start-stop approximation is common to all existing imaging techniques and this is central to the thesis and holds the fundamental difference between the new imaging scheme developed in [2] and current techniques.

1. Linearized Scattering Model by Means of the Born Approximation

Scattering models in the past have been built upon a foundation that views targets as being composed of simple, non-interacting point scatters. When the imaging scene consists of multiple targets, multiple scattering occurs and accounting for this makes the problem extremely complex. For this reason, the "weak scatterer" or Born approximation is used. This approximation is very useful because it makes the imaging problem linear and manageable.

However, the Born approximation has its limitations that may result in image artifacts due to its neglect of the multiple-scattering terms. Actual multiple-scattered waves return to the radar later than expected from the single-scattering model. These waves are then interpreted as having come from an object farther from the radar. In addition, increased capabilities in radar resolution and sensitivity and parallel advancements in computational technology have exposed the inadequacies of such simple scattering models. With the ability of radar systems to resolve and image the *components* (subscatterers) that lie *within* the support of a traditional target, it is inevitable that new radar target models that can describe these multiple scattering effects accurately, whether multiple targets or multiple components of a single target are required. Current approaches typically utilize correction techniques to enhance imaging algorithms based on the low order "weak scatterer" model.

2. Bandwidth Limited Radar Systems

All real systems are bandwidth limited. In addition, radar data is often corrupted by noise. Consequently these limitations induce unwanted image artifacts and reduce image resolution.

3. "Start-Stop" Approximation

In practice, modern pulsed radar systems do not usually measure the Doppler shift. Instead they estimate velocity from the phase difference between returns from successive pulses. Hence, the waveform commonly used by modern radars is a train of high-range resolution pulses that enable pulse-to-pulse velocity estimation. Such waveforms inherently invoke a *start-stop* approximation, which assumes that the target is stationary during the time the radar pulse illuminates the target and moves only between pulses. Because the individual pulses are short and targets of interest are small and move slowly compared to the speed of light, this is almost always a good approximation. Using this approximation, good velocity estimates are based on range-rate (two accurate range measurements, separated by a time interval). However, no Doppler shift measurements are actually measured by the system. From the measured range and range-rate data, spatial images are then formed.

However, in practice there is a limit to the how short a pulse can go. In order to achieve a relatively good signal-to-noise (SNR) ratio by coherent integration, long pulse trains are required. As a result, when the returned pulses are coherently processed at the receiver, the stationary target assumption may no longer hold. The scatterer may move to a different position within that pulse interval or resolution cell and result in a blurred image.

C. MOTIVATION–IMAGING MOVING TARGETS

To date, there have been a number of attempts to develop imaging techniques that can handle moving targets. For example space-time adaptive processing (STAP) is a signal processing technique that was originally developed for detecting slow-moving targets via airborne radars. Multiple-element antenna array together with real-aperture imaging techniques to produce ground moving target indicator (GMTI) images [24] were the key features in STAP. The technique described in [25] together with SAR (designed to image stationary scenes) and GMTI processing develop a new techniques for detecting slow-moving surface targets that exhibit start-stop maneuvers. Another method described in [12] discusses the extension to non-sideways looking array radar.

The concept of velocity synthetic aperture radar (VSAR) is another development described in [10]. VSAR is essentially a multi-element SAR system involving conventional processing to form an image at each element. Here, the image phases are preserved and compared to deduce target velocity. However, VSAR processing assumes that the scatterers remain in a single resolution cell throughout the integration time.

Time-frequency methods are also very useful in the area of image generation. This method, when used for signal analysis, allows decomposition of the frequency spectrum of time-varying signals in shorter time frames and provides an added dimension for examining the dynamic behavior of the signal as it varies over time. The size and shape of the weighting window function can be altered to fit the specific analysis requirement for the signal. Recently, this method was combined with ISAR to improve imaging, motion compensation and micro-Doppler target vibration studies [8 20 and 21]. It was reported in [20] that the time-frequency transform (TFT) was used to construct inverse synthetic aperture radar (ISAR) images of targets with high rotation rate by helping to overcome the migration of individual scattering points from one range cell to another.

However, all these imaging techniques make a common approximation that a target in motion is assumed to be momentarily stationary while interrogated by a radar pulse. Therefore, it is apparent that the need for an imaging scheme that can accommodate target motion during imaging process is necessary and this constitutes a main focus of this thesis.

D. OBJECTIVE

The objective of this project is to study a linearized imaging theory developed by Professors *Cheney* and *Borden* [2] for an imaging scene containing moving targets and this will be done in four parts. Part 1 analyses the Point Spread Function (PSF) focusing on imaging a static point scatterer. This was completed in a previous thesis [3]. Part 2, which is the main focus of this thesis, develops the new imaging code based on a static point scatterer. Part 3 and 4 will further develop the code to cater for different waveforms and applications to real data. In this thesis, the physics involved and the approach for

addressing image artifacts common to targets moving in an unknown fashion will be discussed. The study of the new image model through correlation of the image data to the radar model will also be analyzed and developed via Matlab simulation. This image model will be compared with the corresponding point-spread function to examine the localization in phase-space (position-velocity). The behavior of the imaging model will also be examined under different aperture geometries.

E. THESIS ORGANIZATION

The thesis is organized in the following manner:

Chapter II illustrates the development of radar imaging theory by looking at the basic building blocks necessary for imaging—radar operating principles, scattering models, correlation reception—and how these components translate to imagery. Finally, the thesis includes an overview of the inverse nature of the radar imaging problem to provide better appreciation of issues pertaining to practical measurement systems and how information is extracted from measurements to obtain the best estimates of the object.

Chapter III applies the concepts put forth in Chapter II to the imaging scenario. The discussion here is based on the work of Cheney and Borden [2] in imaging moving targets from scattered waves. The effects of multiple moving targets on the scattering model are described. The approximations invoked, specifically slow-moving, narrow-band, and far-field, are examined. A scattering model to be used in the simulation program will be presented.

Chapter IV will discuss the radar ambiguity function and the relationship between estimation errors and the transmitted waveform. Particular emphasis will be given to image quality analysis and the derivation of the point-spread function to quantify the performance of the imaging scheme developed in Chapter V.

Chapter V examines further implications of the transmitted waveform through the pulse compression perspective. In particular, the Chirp signal is discussed.

Chapter VI demonstrates the behavior of the imaging scheme. A simple simulation program is developed and the results of the simulation, specifically the effect of different aperture geometries, are discussed. This chapter also summarizes the major findings of the thesis work and provides recommendations for future work.

II. IMAGING THEORY

In Chapter II, we will look at some of the basics in imaging theory and examine how spatial images are formed. We begin by examining the physics behind extracting range and Doppler shift (range-rate) information using a radar system. The chapter concludes with a brief look at the inverse nature of the imaging problem and characteristics of measurement systems and some of the issues and challenges pertaining to radar imaging.

A. RADAR SYSTEMS

Radar systems can be classified by two main designs, namely stepped-frequency and pulsed. Most of the fielded radar systems are pulsed systems, as opposed to stepped-frequency systems. There are two key measurements that radar systems make: the strength of the backscattered field and the round-trip delay time of transmitted signal pulse reflected from distant targets. The range from the radar to the target is determined by measuring the time delay (round trip) for the radar pulse to travel to the reflecting target and back. Because the radar pulse travels at the speed of light we can determine the range R from $R = c\tau / 2$ where τ is the round trip time delay.

There are several aspects in understanding how radar signals provide information for imaging. Firstly, is the kind of waveforms that radar uses to transmit a signal. Radar signals are real-valued functions of time but it is convenient to express the waveforms as complex-valued functions. The radar system is able to measure both the amplitude and phase of these signals as functions of time and so a radar signal is of the form $A(t)e^{i\phi(t)}$ the function $\phi(t)$ is the "phase" and provides the phase information. The function $A(t)$ is the "amplitude" and provides the magnitude of the waveform.

All radar waves are electromagnetic waves governed by Maxwell's equations and satisfy the wave equation and radiation condition. Essential target information such as range, speed, and bearing can be extracted from the waveforms.

The resolution in the down-range direction is determined by the pulse duration and the pulse bandwidth. A typical carrier frequency lies in bands that coincide with a low atmospheric attenuation window—1-40GHz. Larger bandwidth will imply finer resolution for imagery in the range direction. The concept of resolution will be addressed in Chapter III.

B. SCATTERING OF ELECTROMAGNETIC WAVES

In this section, we look at the behavior of electromagnetic waves and, in particular, the propagation and scattering of these waves. Knowing the properties of such waves provides important information about the transmitted and received signals and also provides target information. The following two sections will further develop these ideas.

From the discussion in [18], a simple one-dimensional scattering model for a moving PEC[1] plate in free space is a commonly used approximation for a typical radar echo wave. From Maxwell's equations, it can be shown that an electromagnetic wave in the far-field consists of the electric field $\tilde{E}$, magnetic field $\tilde{H}$, and wave vector (direction of propagation) $\hat{k}$. These three vectors are mutually perpendicular. For a transmitted wave with its field component orthogonal to the x-direction with $\hat{k} = \hat{x}$, the boundary condition on the PEC results in the following relationship between the scattered and transmitted electric field:

$$\tilde{E}_{scatt}\, g(t + R(t)/c) = -\tilde{E}_{inc}\, f(t - R(t)/c)$$

This scattered field consists of a left traveling wave (moving in the negative $\hat{x}$-direction) where position of a phase-front is given by $x(t) = R(t)$. Consider a plate that moves linearly in the x-direction, so that $R(t) = x + vt\Big|_{x=R(\text{at boundary})}$. By making use of substitution $u = t + R(t)/c$, we can solve for t in terms of u at the boundary:

[1] A perfect electrical conductor (PEC) allows the charges to move freely and instantaneously in response to a field; consequently the fields inside a PEC are zero. The resulting boundary conditions are: the tangential components of the electric field must be zero and the tangential components of the magnetic field are related to currents flowing on the surface of the PEC.

$$t = \frac{u - R/c}{1 + v/c}$$

and obtain the expression for the scattered field:

$$\tilde{E}_{scatt}\, g(t + R(t)/c) = -\tilde{E}_{inc}\, f\left[\alpha(t + x/c - R/c) - R/c\right] \tag{2.1}$$

where α is the Doppler scale factor:

$$\alpha = \frac{1 - v/c}{1 + v/c} \tag{2.2}$$

For a transmitted field consisting of a signal waveform $s(t)$ mixed with a carrier wave $\cos(\omega_0 t)$, the scattered signal received at the antenna ($x = 0$) is:

$$p_{rec}(t) \approx s(t - 2R/c)\cos\left(\omega_0\left[(1 - 2v/c)(t - R/c) - R/c\right]\right) \tag{2.3}$$

This result is based on the assumption that the argument $\alpha(t - R/c) - R/c \approx t - 2R/c$. We also assumed that the scatterer is moving slowly so that υ / c is small. In addition, we can expand the denominator of Equation 2.2 in a geometric series and approximate α by $1 - 2v/c$. The multiplier of t in the argument of the cosine function is the carrier frequency (relative to the transmitted carrier frequency) shifted by an amount

$$\upsilon = -\frac{2v}{c}\omega_0 \tag{2.4}$$

This is the Doppler shift. As in the stationary scatterer case, the received signal is time-delayed, but there is also a Doppler-shifted version of the transmitted signal.

C. CORRELATION RECEPTION–RADAR DATA MODEL

One of the fundamental requirements for effective radar operation is detection of signals in noise. Radar detects the presence of an echo signal reflected from a target and extracts information about the target for imaging. The conservation of energy requires

that the wave intensity from a finite-sized antenna decreases in strength as the inverse square of the distance. As a result, the round trip signal power received by the radar decays by a factor of $1/R^4$ relative to the signal that was transmitted. For example, at typical radar operating distances, the received power can be as low as 10^{-18} Watts. This problem is further complicated by the presence of thermal noise at the receiver and may result in poor image formation.

There are many ways to overcome this problem for example, increasing the power of the transmitter can help to increase the signal-to-noise ratio (SNR), but there are practical limits to relying solely on this approach. Coherent integration of multiple pulses is another method, but the main practical effect of an increased pulse repetition frequency decreases during the maximum unambiguous range, and the fact that targets motion during data collection and pulse integration alters the phase of the scattered field. Hence, the subsequent discussion examines the idea of correlation comparison performed coherently so that the phase of the transmitted signal is preserved in the reference signal.

One way to allow coherent correlation is to transmit long coded pulses, together with appropriate signal processing techniques called *matched filtering* or *correlation reception.* This is known as pulse compression (see Chapter V). The correlation receiver or matched filter is an important example of a radar signal processor for detection of desired signals. The output of the matched filter is the cross-correlation function of the received signal and the expected received signal, corresponding to the transmitted signal. Hence, there will be a mathematical equivalence between the correlation receiver and the match filter receiver, and it is possible to implement the matched filter as a correlation process.

Correlation reception introduces an intuitive approach for developing the standard radar data model used in imaging and the result is optimal detection in additive noise. For example, with a presence of Gaussian noise, correlation reception will select the best-guess estimate for the radar signal associated with the field reflected from a target, the scattered signal $s_{scatt}(t)$. From [19], we can see that such processing, when averaged over all time reduces to finding a function $s_{scatt}(t)$ that minimizes:

$$\int_{-\infty}^{\infty} \left|s_{rec}(t')\right|^2 dt' + \int_{-\infty}^{\infty} \left|s_{scatt}(t')\right|^2 dt' - 2\,\mathrm{Re}\int_{-\infty}^{\infty} s_{rec}(t')s_{scatt}^{*}(t')dt' \tag{2.5}$$

The key to this approach is to determine $s_{scatt}(t)$ from the random measurements of $s_{rec}(t)$. The first two terms are system-scenario specific. Searching for the best minimizing function hinges on the last term and can be made more efficient by restricting the search to a few parameters derived from some model. In this case, the natural model is based on the scattering interaction between the interrogating field and the target. If $s_{inc}(t)$ denotes an incident pulse transmitted by the radar, then the linear radar (weak-scatterer) scattering model follows by superposition

$$s_{scatt}(t) = \iint_{-\infty}^{\infty} \rho(\upsilon,\tau)s_{inc}(t-\tau)e^{i\upsilon(t-\tau)}d\tau d\upsilon \tag{2.6}$$

where $\rho(\upsilon,\tau)$ is the target reflectivity density for a radar system that measures two parameters, range and radial velocity. This reflectivity density is defined in such a way that $\rho(\upsilon,\tau)d\tau d\upsilon$ is proportional to the field reflected from the target at range between $c\tau/2$ and $c(\tau+d\tau)/2$ with Doppler shift between υ and $\upsilon+d\upsilon$.

From Equation 2.6, the scattered field is naturally modeled by the two parameters τ and υ. The search space will be parameterized by the time shift τ and the frequency shift υ. Considering the last term of Equation 2.5 and maximizing for all τ, υ in the scattered model, the correlation integral is:

$$\eta(\upsilon,\tau) = \int_{-\infty}^{\infty} s_{rec}(t')s_{inc}^{*}(t'-\tau)e^{-i\upsilon(t'-\tau)}dt' \tag{2.7}$$

This correlation integral seeks out the component of the received signal that "matches" the time-delayed, frequency-shifted version of the transmitted signal. Unlike signals will be suppressed and, consequently, correlation receivers attempt to find the τ and υ that maximize the real part of Equation (2.7). The expected output of the correlation receivers is obtained by substituting Equation (2.6) into the correlation integral of Equation (2.7).

$$\eta(\upsilon,\tau)=\iiint_{-\infty}^{\infty}\rho(\upsilon',\tau')s_{inc}(t'-\tau)s_{inc}^{*}(t'-\tau')e^{i\upsilon(t'-\tau)}e^{-i\upsilon(t'-\tau')}dt'\,d\tau'\,d\upsilon' \tag{2.8}$$

Notice that in Equation 2.8 the correlation noise term has been suppressed. The correlation noise term, which is the correlation integral between random noise and the time-delayed, frequency-shifted version of the transmitted signal measures how well the scattered signal matched the random noise will usually be small for coherent systems. Rearranging Equation 2.8,

$$\eta(\upsilon,\tau)=\iint_{-\infty}^{\infty}\rho(\upsilon',\tau')\chi(\upsilon-\upsilon',\tau-\tau')e^{i\frac{1}{2}(\upsilon+\upsilon')(\tau-\tau')}d\tau'\,d\upsilon' \tag{2.9}$$

where

$$\chi(\upsilon,\tau)=\int_{-\infty}^{\infty}s_{inc}(t'-\frac{1}{2}\tau)s_{inc}^{*}(t'+\frac{1}{2}\tau)e^{i\upsilon t'}dt' \tag{2.10}$$

Equation 2.9 is the standard radar data model and it describes the output of the correlation receiver as the convolution of ρ and χ up to a phase factor. The function $\chi(\upsilon,\tau)$ defined by Equation 2.10 is the radar ambiguity function. Radar imaging is closely related to the radar ambiguity function that characterizes the accuracy of the target position and radial velocity from the radar data (see Chapter III).

D. ONE-DIMENSIONAL (HIGH RANGE RESOLUTION) IMAGING

One-dimensional imaging involves the generation of range profiles, which can be used to describe target substructure. For high range resolution (HRR) techniques, the transmitted pulse's instantaneous range resolution is smaller than that of the target. As it sweeps across the target, it sequentially excites the target's scattering sub-elements, which re-radiate energy back to the receiver. When these scattering sub-elements are non-interacting and point-like, the scattered pulse will be a sum of damped and blurred images of the incident pulse, which are shifted by time-delays that are proportional to the sub-element's range [1]. Figure 1 shows an example of one-dimensional images created

the HRR radar systems. It can be observed that the profile displays additional peaks outside of the target support, clear evidence of the problem associated with a single, non-interacting scatterer approximation.

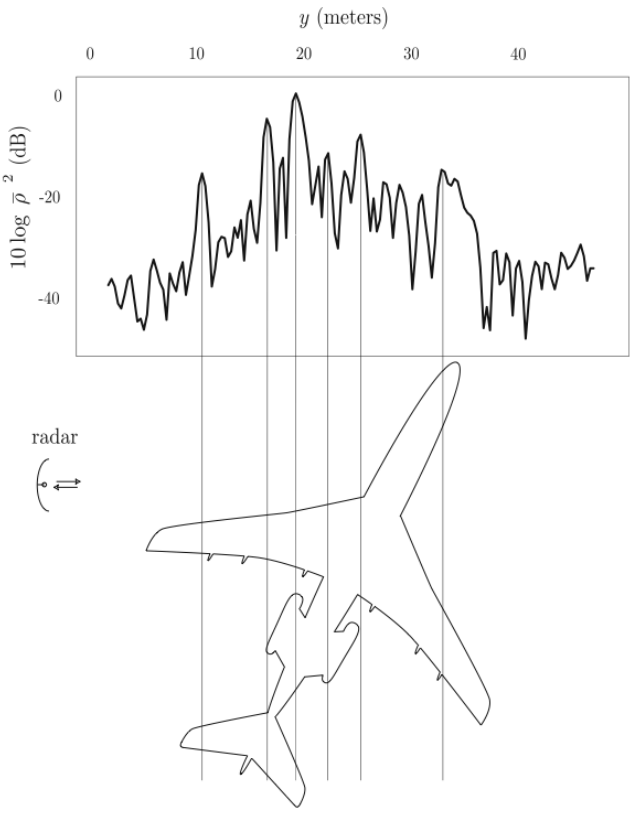

Figure 1. Example of a range profile from a B-727 jetliner. The top view (with orientation at time of measurement) is displayed beneath. From [1].

The signal received from a distribution of non-interacting, stationary targets can be modeled as

$$s_{rec}(t) = \int_{-\infty}^{\infty} \rho(\tau') s_{inc}(t - \tau') d\tau' + n(t) \tag{2.11}$$

where $n(t)$ represents an additive and random noise term. Application of a matched filter to obtain the radar data model used for imaging

$$\eta(\tau) = \int_{-\infty}^{\infty} s_{rec}(t')s_{inc}^{*}(t'-\tau)dt' = \int_{-\infty}^{\infty} s_{inc}^{*}(t'-\tau)\int_{-\infty}^{\infty} \rho(\tau')s_{inc}(t'-\tau')d\tau' dt' \quad + \quad \text{noise term}$$

$$= \iint_{-\infty}^{\infty} s_{inc}^{*}(t'-\tau)s_{inc}(t'-\tau')dt'\rho(\tau')d\tau' \quad + \quad \text{noise term}$$

Making the substitution $t'' = t' - \tau'$ and neglecting the noise term (negligible with matched filtering) gives

$$\eta(\tau) = \int_{-\infty}^{\infty} \chi(\tau - \tau')\rho(\tau')d\tau' \tag{2.12}$$

where χ is the autocorrelation

$$\chi(\tau) = \int_{-\infty}^{\infty} s^{*}(t''-\tau)s(t'')dt'' = \int_{-\infty}^{\infty} s^{*}(t')s(t'+\tau)dt' \tag{2.13}$$

Equation 2.12 represents a one-dimensional image and shows how the true distribution ρ is related to the radar data model. The image is the convolution of ρ with χ, which in high-range resolution imaging is also commonly referred to as the *point-spread function* (PSF). The point spread function obtains its name from the fact that if ρ consists of a single point $\delta(t)$, then the image is $\eta(t) = \int \chi(t-t')\delta(t')dt' = \chi(t)$. Thus, χ quantifies the degree to which a single point appears spread out in the HRR image.

The down-range profile can be affected by a variety of factors such as the target aspect angle, position of the scatterers, or masking of scatterers by other parts of the target. Additionally, while the use of short pulses enhances the resolution, it concurrently leads to large bandwidth requirements. Wide bandwidths can increase system complexity and increase the likelihood of interference from other emitters in the electromagnetic spectrum. A short-pulse waveform also provides less accurate radial velocity measurement, a natural consequence from the properties of the radar ambiguity function (More details on radar resolution and the ambiguity function in Chapter III). An important implementation limitation in practical radar applications is the required high peak power to transmit short pulses over long ranges. High peak power transmission can

be problematic, especially at high frequencies due to the small waveguide dimensions and the small area of the anodes of the microwave sources.

Radar target recognition using only range profiles has limited applications. This is because a range profile will not be able to distinguish cross-range target structures. All scatterers located at the same distance from the radar will reflect energy back to the radar with the same time delay. Hence, when the radar illuminates many distinct targets at any instant, meaningful interpretation of on-scene target (multiple) disposition cannot be derived based on a set (single) of range-only data.

E. TWO-DIMENSIONAL IMAGING

In order to interpret a target more effectively, additional information is needed on top of the range profile. This information can be in the form of a high-resolution cross-range profile, a Doppler profile, or simply the "triangulation" of range profiles.

As a simple illustration for extension of the radar imaging concept to two dimensions, "triangulation" of different sets of range profiles will be explained (Figures 2 and 3). This approach enables the determination of cross-range target structures while using only HRR radar systems and relies on collecting multiple sets of range profiles from different target orientations, processing them, and subsequently synthesizing a two-dimensional image.

A simple example is used to illustrate this approach. Consider a set of three point targets with the radar located at the same distance from target 2 and 3 in Figure 2. When the geometry is oriented as shown, the return echo will only indicate two targets. Hence, ambiguity exists when targets lie along the bands of constant range from the radar.

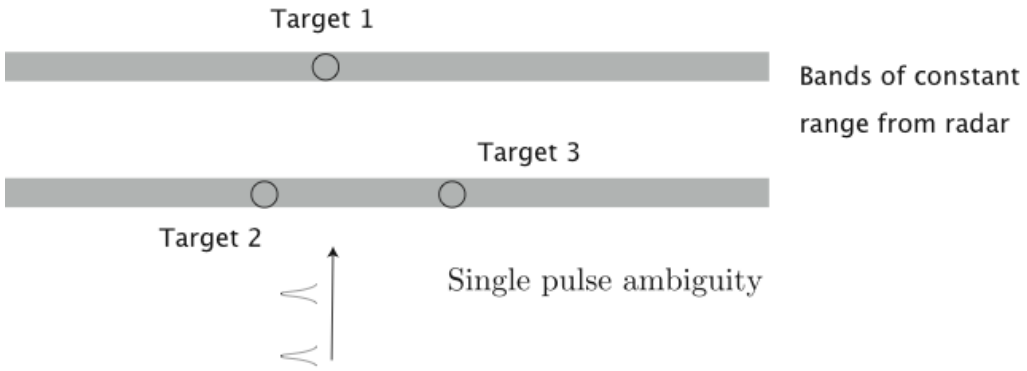

Figure 2. Ambiguous scenario from a single radar pulse. From[19].

Using multiple sets of data taken from different directions, triangulation will allow for gradual buildup of the relative positions of the three targets, as shown in Figure 3. The range profiles are swept in the cross-range direction to form bands of constant range from the radar; these bands represent the possible locations of the target scatterers. The crossing points of these bands are used to determine the scattering center locations. The success of such an imaging scheme hinges fundamentally on the ability to correlate or correctly superimpose the various constant range bands. Otherwise, the intersection of the swept lines will be mistaken, resulting in image artifacts.

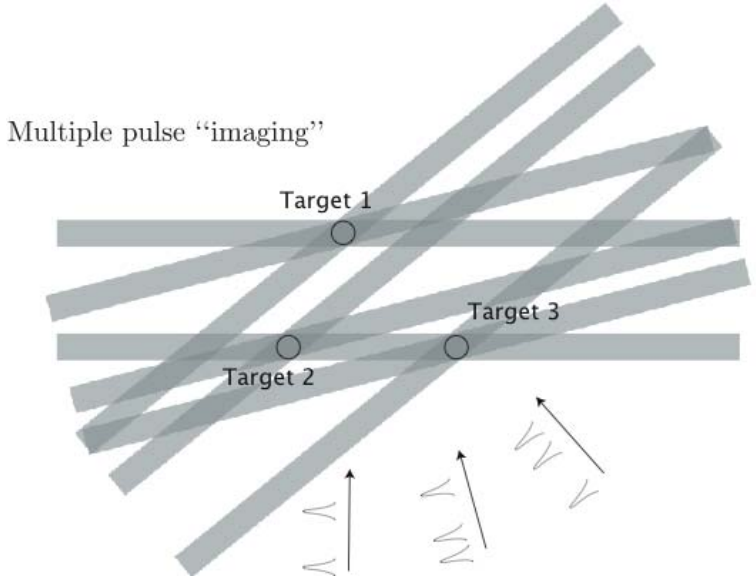

Figure 3. Cross-range information obtained from range profiles. From [19].

When a radar system is used for imaging a moving target, the received signal is a time-delayed and Doppler-shifted version of the transmitted signal. The measured echo signal from a single point-like moving target can be expressed as

$$s_{rec}(t) = \rho s_{inc}(t-\tau)e^{-i\upsilon(t-\tau)} + n(t) \tag{2.14}$$

Because there are two unknown parameters to estimate, namely the delay τ and the Doppler shift υ, a single matched filter will no longer be enough. A set of matched filters, one for every possible Doppler shift, will have to be applied as

$$\eta(\tau,\upsilon) = \int_{-\infty}^{\infty} h_{\upsilon}(t-t')s_{rec}(t')dt' = \rho\int_{-\infty}^{\infty} h_{\upsilon}(t-t')s_{inc}(t'-\tau)e^{-i\upsilon(t'-\tau)}dt' \ + \text{ noise term}$$

in order to estimate τ and υ. Estimated values occur where $|\eta|$ takes on its maximum. For a distribution of non-interacting moving targets, the output from the filter bank is

$$\begin{aligned}
\eta(\tau,\upsilon) &= \int_{-\infty}^{\infty} s_{inc}^{*}(t'-\tau)e^{-i\upsilon(t'-\tau)}s_{rec}(t')dt' \\
&= \int_{-\infty}^{\infty} s_{inc}^{*}(t'-\tau)e^{-i\upsilon(t'-\tau)}\iint_{-\infty}^{\infty} \rho(\tau',\upsilon')s_{inc}(t'-\tau')e^{-i\upsilon'(t'-\tau')}d\tau' d\upsilon' dt' \\
&= \iiint_{-\infty}^{\infty} s_{inc}^{*}(t'-\tau)e^{-i\upsilon(t'-\tau)}s_{inc}(t'-\tau')e^{-i\upsilon'(t'-\tau')}dt'\,\rho(\tau',\upsilon')d\tau' d\upsilon' \\
&= \iiint_{-\infty}^{\infty} s_{inc}^{*}(t''+\tau'-\tau)e^{-i\upsilon(t''+\tau'-\tau)}s_{inc}(t'')e^{-i\upsilon'(t'')}dt''\,\rho(\tau',\upsilon')d\tau' d\upsilon' \\
&= \iint_{-\infty}^{\infty} \chi(\tau-\tau',\upsilon-\upsilon')e^{-i\upsilon'(\tau-\tau')}\rho(\tau',\upsilon')d\tau' d\upsilon'
\end{aligned} \tag{2.15}$$

where

$$\chi(\tau,\upsilon) = \int_{-\infty}^{\infty} s_{inc}^{*}(t''+\tau)e^{-i\upsilon(t'')}s(t'')dt'' = \int_{-\infty}^{\infty} s_{inc}^{*}(t'+\tau)s_{inc}(t')e^{-i\upsilon t'}dt' \tag{2.16}$$

is the *radar ambiguity function*. Similar to the one-dimensional case, the ambiguity function can be interpreted as an imaging point-spread function for range-Doppler imaging. Analysis of the ambiguity function determines the fidelity of the range-Doppler imaging process and consequently the accuracy of target range and velocity estimation.

1. Range-Doppler Spatial Image

Range and range-rate measured from radar returns can be interpreted to form spatial images. The following example will illustrate this, provided the relative motion between the antenna and the target is known. Consider a simplified two-dimensional geometry between the radar and target as shown in Figure 4. The target is assumed to have translational and rotational motion only in the two-dimensional plane relative to a stationary radar platform.

Consider a rotating target [18]. For simplification, assume that any overall translational motion is removed.

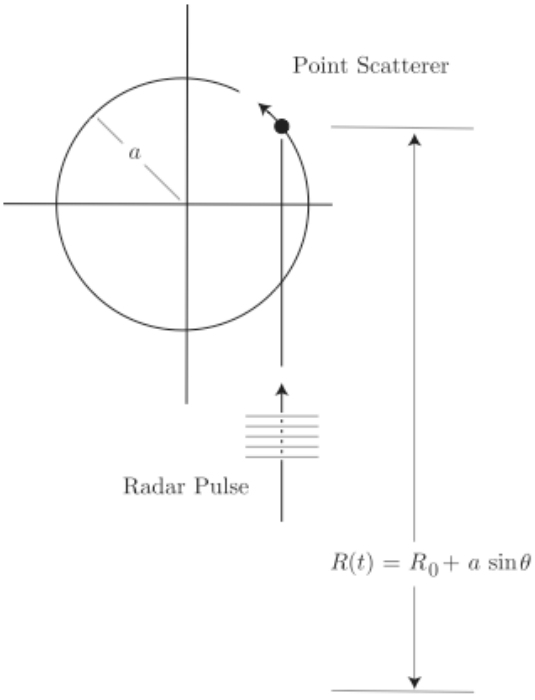

Figure 4. The geometry for locating a point target known to be rotating. From [18].

A point target rotates counter-clockwise in geometry in which the antenna is in the plane of rotation (Figure 4). The coordinate origin coincides with the center of rotation and the center of rotation is a large distance R_0 from the radar antenna. The large range approximation means that the incident wave is approximately a plane wave.

Consequently, all horizontal points are approximately at the same range. If the target is positioned at $(x, y) = a(\cos\theta, \sin\theta)$, then its range is

$$R = R_0 + y = R_0 + a\sin\theta \tag{2.17}$$

If its angular velocity is $\dot{\theta} = d\theta / dt$, then its velocity vector is $a\dot{\theta}(-\sin\theta, \cos\theta)$, its tangential speed is $|\upsilon| = a\dot{\theta}$, and the down-range ($y$) component of the velocity is $\dot{R} = |\upsilon|\cos\theta = a\dot{\theta}\cos\theta$. However, since $x = a\cos\theta$, this down-range velocity can be written $\dot{R} = x\dot{\theta}$, where x is the cross-range component of the position. Note that for $x > 0$, the down-range velocity is negative, whereas for $x < 0$, it is positive.

This means that because a radar system can measure range $(R_0 + y)$ and range-rate $(\dot{R} = x\dot{\theta})$, it can determine the (x, y) location of the point in space provided $\dot{\theta}$ is known. In particular, the radar measures the time delay $\tau = 2R / c$ and the Doppler shift

$$\upsilon_D = -\frac{2\dot{R}}{c}\upsilon_0 = -\frac{2x\dot{\theta}}{c}\upsilon_0$$

which means that the coordinates of the point are given by

$$(x, y) = (-\frac{\upsilon_D}{\upsilon_0}\frac{c}{2\dot{\theta}},\ \frac{c\tau}{2} - R_0) \tag{2.18}$$

This example shows how the range-rate radar measurements can be used to estimate Doppler and cross-range information. Further, the simple example highlights the difficulties in practical implementation of the radar scattering model. Estimates of the scattered field require any variations in range $\hat{R}$ to be estimable. While it is reasonable to assume in the one-dimensional imaging methods that $\hat{R}$ is constant over the data set, this is not true for the two-dimensional imaging schemes. $\hat{R}$ will generally vary due to the target (translational) motion that occurs during measurements made while the target

rotates. The effect of failing to correctly account for this translational motion will be the introduction of phase errors into these data and a source of image corruption.

F. RADAR IMAGING—AN INVERSE PROBLEM

A discussion of imaging theory will not be complete without addressing the inverse nature of the imaging problem and its associated issues. As this thesis is focused primarily on developing and analyzing the point spread function rather than imaging, the intent of this section is to highlight the key characteristics of such inverse problems—issues pertaining to practical measurement systems and how information is typically extracted from measurements to obtain the best estimates of the target object.

Radar scattering can be well-approximated by a linear, shift-invariant system. This is an important characteristic, as it states that the object function $f(x)$ at each point x has a corresponding output image $m(x)$. Further, the system will measure objects the same no matter when they start or, equivalently, where they are located. Radar imaging will not be meaningful if the delayed version of the target looks different for different delays. A general formulation of the imaging problem can be achieved by considering an imaging system represented by the functional operator or "kernel" κ that describes how the measurement system works

$$m = \kappa f \tag{2.19}$$

The *direct problem* in radar imaging refers to the mapping from the target to the quantities that can be measured by the radar. Consequently, the *inverse problem* is concerned with "reproducing" the original target from given data and knowledge of the direct problem; in the case of radar imaging, it will be radar measurements and knowledge of the scattering model.

1. Well-Posed and Ill-Posed Problems

One of the issues for inverse problems is their ill-posed nature. An ill-posed problem is one whose solution is not unique and/or does not exist for any data and/or does not depend continuously on the data. In the case of a band-limited system, the

solution of the inverse problem is not unique. This is because the imaging system does not transmit information about the target at frequencies outside the band of the measuring system.

Consider discretized measurement systems in which the measurements are collected at specific points, and so Equation 2.19 can be written in matrix form. The basic goal of getting a good estimate $\bar{f}$ from the measurements m can be notionally represented as

$$\bar{f} = \kappa^{-1} m \tag{2.20}$$

It can be observed that κ, which represents the measurement system, imposes certain properties on the measurement system. In general, the matrix κ is $N \times M$ ($M > N$) as the object function is infinitely dimensional and will not be confined to the limitations of the measurement system. Consequently, Equation 2.20 has more unknowns than there are linearly independent equations and so the system cannot have a unique solution.

Since the object space (M-dimensional) is typically larger than the measurement space (N-dimensional), there exists what is known as the nullspace, which consists of all vectors $f - \kappa f$ or, physically, all the things that *cannot be measured*. Null space accounts for measurement artifacts and is determined by the kernel κ.

The accepted approach for solving inverse problems that are ill-posed is to search for approximate solutions satisfying additional constraints based on the physics of the problem [22]. This set of approximate solutions corresponding to the same data function is the set of objects with images close to the measured one and is expressed in what are known as the "normal equations"

$$\kappa^T \kappa \bar{f} = \kappa^T m \tag{2.21}$$

2. Data Reconstruction—Regularization

Equation 2.21 specifies the set of conditions that must be satisfied by the least-squares solution $\bar{f}$ which can be rewritten as

$$\bar{f} = (\kappa^T \kappa)^{-1} \kappa^T m \tag{2.22}$$

Recall that the measured data suffers from finite dimension and noise contamination. These are problems since $(\kappa^T \kappa)$ is poorly conditioned and the effect of noise is magnified (i.e. errors increase) as the dimensionality of the problem gets larger. Two techniques will be highlighted here, namely the singular value decomposition (SVD) and Tikhonov regularization, to mitigate the effects of noise when estimating $\bar{f}$.

From linear algebra methods, the matrix $(\kappa^T \kappa)^{-1} \kappa^T$ can be expressed in terms of its SVD [19]:

$$(\kappa^T \kappa)^{-1} \kappa^T = UDV^T \tag{2.23}$$

where the matrices *U*, *V* contain the eigenvectors of $(\kappa^T \kappa)$, and *D* will have diagonal elements of the form $1/\sqrt{\lambda_i}$ (where λ_i are the corresponding, non-zero eigenvalues). A consequence of the kernel κ being bounded is that the eigenvalues necessarily form a sequence that gets arbitrarily close to zero as the number of measurements increase. The diagonal elements of *D* get large when higher dimensional data are used, and if the data are contaminated by noise, it follows from Equations 2.22 and 2.23 that noise will also be multiplied by a large value. Hence, one simple approach to mitigate the noise effect is to truncate the SVD representation when λ_i falls below some chosen threshold value. The corresponding diagonal element is set to zero. This method is known as the *truncation filter*.

Tikhonov regularization modifies $(\kappa^T \kappa)^{-1} \kappa^T$ to a matrix with better condition number by adding a fixed scalar α to the original normal equations. Equation 2.22 can then be rewritten in the form

$$\bar{f} = (\kappa^T \kappa + \alpha I)^{-1} \kappa^T m \tag{2.24}$$

When $\alpha = 0$, the original normal equations are returned and so it can be expected that small values of α will not change the system description too much.

After introducing α, the diagonal elements of *D* in Equation 2.23 become

$$D_{ii} = \frac{\sqrt{\lambda_i}}{\lambda_i + \alpha} \tag{2.25}$$

when $\lambda_i >> \alpha$, $D_{ii} \approx 1/\sqrt{\lambda_i}$ (as before). When $\lambda_i = \alpha$, however, $D_{ii} \approx \sqrt{\lambda_i} / \alpha$ and will not become arbitrarily large. Consequently, the noise problem is moderated.

THIS PAGE INTENTIONALLY LEFT BLANK

III. IMAGING DATA MODEL

So far we have discussed the different types of imaging theories and techniques used for radar imaging. This chapter will make use of these ideas and concepts to develop an approach to imaging moving targets from scattered waves. We will also be looking at the three-dimensional case in order to develop the imaging model.

A. INTEGRAL EQUATION APPROACH TO SCATTERING

From the previous chapter, we have seen that for the one-dimensional scattering problem from a moving plate, the signal that returns to the radar is a time-delayed and frequency-shifted version of the transmitted signal. This is also the case for three-dimensional scattering from a moving, point-liked target. A point target is the traditional model used for developing imaging analysis and will also be used for the thesis. The representation of a target as points is appropriate because for high-frequency waveforms scattered from smooth conducting surfaces, the net scattering effects from the surface is equivalent to the contribution from the entire series of points known as specular points [19].

Applying traditional electromagnetic approaches to scattering will typically involve solving a differential wave equation and imposing the appropriate boundary conditions at the surface of the scatterer. However, for realistic radar targets, this process is difficult to implement because there is no coordinate system that can represent the boundary conditions for complex targets.

Therefore it is convenient to reformulate the scattering problem. From the mathematical approach, it turns out that there is an equivalent integral equation for every differential equation, and this integral equation can inherently incorporate any boundary conditions in the solution.

This concept can be explained as follows: take a scattering object to be located in free space with an index of refraction $n(x)$. Using a monochromatic wave, with harmonic time dependence, illuminate on an object. The reduced wave equation of the field becomes

$$\nabla^2\Psi(x) + k^2 n^2(x)\Psi(x) = 0 \tag{3.1}$$

This is also known as the Helmholtz equation and *k* is the wave number in free space. Note also that $n(x) \neq 1$ on the scatterer. By splitting the field Ψ into the incident field Ψ_{inc} which is the incoming wave, and the scattered field Ψ_{scatt}, Equation 3.1 can be simplified to

$$\begin{aligned} &\nabla^2\Psi_{scatt}(x) + k^2\Psi_{scatt}(x) = k^2(1-n^2(x))\left(\Psi_{inc}(x) + \Psi_{scatt}(x)\right) \\ &\equiv \rho(x)\left(\Psi_{inc}(x) + \Psi_{scatt}(x)\right) \end{aligned} \tag{3.2}$$

where the scattering density $\rho(x) = k^2\left(1-n^2(x)\right)$ is a source factor completely determined by the index of refraction of the scatterer *and is zero outside of the scatterer.*

The solution to Equation (3.2) can be obtained based on the application of *Green functions*, and we can write the solution as

$$\Psi_{scatt}(x) = \iiint_D G_k(x',x)\rho(x')\left(\Psi_{inc}(x') + \Psi_{scatt}(x')\right)d^3x' \tag{3.3}$$

This is a *Lippmann-Schwinger* equation. It can be observed that the problem of solving Equation 1.1 has been reduced to finding the Green function $G_k(x',x)$ *in free space* (*k* denotes a specific frequency). The scattered field is also written as an integral over the *scatterer D* since $\rho(x) = 0$ otherwise, and hence automatically satisfies the required boundary conditions for a known target.

It is also important to note that there are several aspects to the *Lippmann-Schwinger* equation:

(1) There are generally many functions that can serve as Green functions $G_k(x',x)$ *in free space*. While there are no bounding surfaces other than those defined by the scattering object, we are interested in $G_k(x',x)$ that obey the Sommerfeld radiation condition $\lim_{r\to\infty} G_k(x',x) \propto \frac{1}{r}$ as this is more applicable to the typical radar operations.

(2) The *inverse* scattering problem, i.e. that of determining ρ given Ψ_{inc} and Ψ_{scatt}, can also be approached using the *Lippmann-Schwinger* equation as a model for Ψ_{scatt}.

B. LINEARIZED DATA MODEL (TIME-VARYING SYSTEMS)

Besides using the integral equation approach to solve the scattering problem, there is also a need to make the appropriate approximation in order for the radar model to be tractable. By enforcing the Born or "weak scatterer" approximation, where the object distribution (cell) is not self-interacting, multiple scattering events are treated as negligible in comparison with the primary scattering events. The result of this is a linearized (approximate) data model as follows:

$$\Psi_{scatt}(x) = \iiint_D G_k(x',x)\rho(x')\Psi_{inc}(x')d^3x' \tag{3.4}$$

Equation 3.4 turns out to be a solution for Helmholtz's equation. A typical radar operation is a time-varying problem, and so the time-dependent wave equation and the time-domain Green function will have to be incorporated with the model

$$G_k(x',x) \to g(x',x;t',t) = \frac{\delta(t-t'-|x'-x|/c)}{4\pi|x'-x|} \tag{3.5}$$

With a signal $s_y(t)$ transmitted from position *y* at starting time $-T_y$, the incident field at *x* is

$$\psi_{inc}(x,t) = -\frac{s_y(t+T_y-|x-y|/c)}{4\pi|x-y|} \tag{3.6}$$

Substituting the incident field (Equation 3.6) and the time-domain Green function (Equation 3.5) to Equation 3.4, we get the scattered field $\psi_{scatt}(y,z,t)$ at time *t* and position *z*

$$\psi_{scatt}(y,z,t) = \iint \frac{\delta(t-t'-|z-x'|/c)}{4\pi|z-x'|} \frac{\ddot{S}_y(t'+T_y-|x'-y|/c)}{4\pi|x'-y|} \rho(x')d^3x'dt' \qquad (3.7)$$

where $\ddot{S}_y$ denotes the second time derivative of incident signal $s_y(t)$ and enters as a consequence of the second time derivative in the wave equation. Hence, as a result of the Born approximation and the usage of time-domain Green function, we obtain a linearized data model (Equation 3.7)

C. REFLECTIVITY FUNCTION FOR MOVING TARGETS

Recall that the reflectivity functions $\rho(x)$, or scattering density function first introduced in Equation 3.2 is determined by the target. It is a scale factor of the received signal strength and an important characteristic of radar imaging. For a moving target, a time-varying reflectivity function $\rho(x,t)$ will be used. When the imaging scene contains multiple moving targets or scatterers, the scattering model can be modified as follows:

Let $\rho_v(x-vt)d^3xd^3v$ be the scatterers in the volume element d^3xd^3v of phase space centered at position *x* and velocity *v*. Choose T_y, the time when the signal is first send out, to be such that the scattering density $\rho_v = \rho_v(x)$. This means that all the targets in the scene moves with velocity *v* at time *t=0* (i.e., the signal is transmitted from the transmitter antenna at time $t=-T_y$). As a result, the spatial scatterer density centered at time *t* and position *x* is

$$\rho(x) = \int \rho_v(x-vt)d^3v \qquad (3.8)$$

and the scattered field becomes

$$\psi_{scatt}(y,z,t)=\iiint \frac{\delta(t-t'-|z-x'|/c)}{4\pi|z-x'|}\times\frac{\ddot{S}_y(t'+T_y-|x'-y|/c)}{4\pi|x'-y|}\rho_v(x'-vt')d^3vd^3x'dt' \quad (3.9)$$

In order to simplify the problem, making a change in variables $x'\rightarrow x=x'-vt'$ can change the frame of reference in which the scatterer ρ_v is fixed. As a result the scattered field is modified to

$$\psi_{scatt}(y,z,t)=\iiint \frac{\delta(t-t'-|x+vt'-z|/c)}{4\pi|x+vt'-z|}\times\frac{\ddot{S}_y(t'+T_y-|x+vt'-y|/c)}{4\pi|x+vt'-y|}\rho_v(x)d^3vd^3xdt' \quad (3.10)$$

The data model, or scattered field, is now modified to incorporate moving targets. The physical interpretation to Equation 3.10 is that the wave that emanates from radar transmitter position *y* at time $-T_y$ encounters a target at time t'. This target, during the interval $[0,t']$, has moved from *x* to $x+vt'$. The wave scatters with strength $\rho_v(x)$ and then propagates from position $x+vt'$ to *z*, arriving at time *t*.

To further simplify the equation, let

$$\boldsymbol{R}_{x,z}(t)=x+vt-z, \qquad R=|\boldsymbol{R}|, \qquad \hat{\boldsymbol{R}}=\boldsymbol{R}/R$$

Substituting this to the scattered field Equation 3.10 gives

$$\psi_{scatt}(y,z,t)=\iiint \frac{\delta(t-t'-R_{x,z}(t')/c)}{4\pi R_{x,z}(t')}\times\frac{\ddot{S}_y(t'+T_y-R_{x,y}(t')/c)}{4\pi R_{x,y}(t')}\rho_v(x)d^3vd^3xdt' \quad (3.11)$$

The variable *t'* in the argument of the delta function appears in several terms making it difficult to carry out the integral over *t'*. To address this, let $t'=\bar{t}_{x,v}(t)$ denote the implicit solution of

$$t-t'-R_{x,z}(t')/c=0, \qquad \text{i.e.,} \quad t-\bar{t}_{x,v}(t)-R_{x,z}(\bar{t}_{x,v}(t))/c=0$$

Then, performing the integration over t' yields

$$\psi_{scatt}(y,z,t) = \iint \frac{\ddot{S}_y\left(\bar{t}_{x,v}(t) + T_y - R_{x,y}(\bar{t}_{x,v}(t))/c\right)}{(4\pi)^2 R_{x,z}(\bar{t}_{x,v}(t)) R_{x,y}(\bar{t}_{x,v}(t))} \rho_v(x) d^3v d^3x$$

Substituting $\bar{t}_{x,v}(t) = t - R_{x,z}(\bar{t}_{x,v}(t))/c$ for the first occurrence of $\bar{t}_{x,v}(t)$ in this last equation allows for a more symmetric version

$$\psi_{scatt}(y,z,t) = \iint \frac{\ddot{S}_y\left(t + T_y - R_{x,z}(\bar{t}_{x,v}(t))/c - R_{x,y}(\bar{t}_{x,v}(t))/c\right)}{(4\pi)^2 R_{x,z}(\bar{t}_{x,v}(t)) R_{x,y}(\bar{t}_{x,v}(t))} \rho_v(x) d^3v d^3x \qquad (3.12)$$

D. FURTHER SIMPLIFYING APPROXIMATIONS

Equation 3.12 applies to very general scenarios. It applies to rapidly moving targets without the need for start-stop approximation, and it is appropriate for any transmitted waveforms.

However, this model still has "retarded-time" problems. These problems arise as a consequence of the definition of retarded time $\bar{t}_{x,v}(t)$, which is the delay between the scattered fields reflected from the target to the radar receiver. The retarded time is expressed as $\bar{t}_{x,v}(t) = t - R_{x,z}(\bar{t}_{x,v}(t))/c$ where t is the time when the scattered field reached the radar receiver. Hence, a more accurate result can be obtained when the scatterers are known to be moving in such a way that $R_{x,z}(t)$ can be expanded in a Taylor series around *t=0* and approximated by retaining only the terms linear in *t*— i.e., when the scatterer is "slow moving".

1. Slow-Mover Approximation

Assume that $(|v|t)$ and $(|v|^2 t^2 \times \omega_{\max}/c)$ are much less than $|x-z|$ and $|x-y|$**,** where $\omega_{\max}$ denotes the maximum angular frequency of the transmitted signal s_y. In this case,

$$R_{x,z}(t) = |z - (x - vt)| = R_{x,z}(0) + \hat{\boldsymbol{R}}_{x,z}(0) \bullet vt + \ldots$$

where $\boldsymbol{R}_{x,z}(0) = \boldsymbol{x} - \boldsymbol{z}$, $R_{x,z}(0) = |\boldsymbol{R}_{x,z}(0)|$, and $\hat{\boldsymbol{R}}_{x,z}(0) = \boldsymbol{R}_{x,z}(0) / R_{x,z}(0)$. Substituting this result into the definition of retarded time yields

$$\bar{t}_{x,v}(t) \approx t - \left(R_{x,z}(0) + \hat{\boldsymbol{R}}_{x,z}(0) \bullet \boldsymbol{v} \bar{t}_{x,\upsilon}(t) \right) / c \approx \frac{t - R_{x,z}(0)/c}{1 + \hat{\boldsymbol{R}}_{x,z}(0) \bullet \boldsymbol{v} / c}$$

Inserting this approximation into the result for $\psi_{scatt}(y,z,t)$ yields

$$\psi_{scatt}(y,z,t) = \iint \frac{\ddot{\tilde{S}}_y \left(\alpha_{x,v} \left[t - R_{x,z}(0)/c \right] - R_{x,y}(0)/c + T_y \right)}{(4\pi)^2 R_{x,z}(0) R_{x,y}(0)} \rho_v(x) d^3v d^3x \qquad (3.13)$$

where

$$\alpha_{x,v} \equiv \frac{1 - \hat{\boldsymbol{R}}_{x,y}(0) \bullet \boldsymbol{v} / c}{1 + \hat{\boldsymbol{R}}_{x,z}(0) \bullet \boldsymbol{v} / c} \qquad (3.14)$$

is the Doppler scale factor. Similar to the traditional Doppler shift, it is closely related to the velocity component in target-transmitter direction.

2. Slow-Mover and Narrow-Band Approximation

Typical systems are narrow-band for which the transmitted signal is of the form

$$s_y(t) = \tilde{S}_y(t) e^{-i\omega_y t}$$

where $\tilde{S}_y(t)$ is slowly varying (as a function of *t*) in comparison with $e^{-i\omega_y t}$, where ω_y is the carrier frequency for the transmitter at position *y*. In this case, the time derivatives of s_y are dominated by the $e^{-i\omega_y t}$ factor, and $\ddot{\tilde{S}}_y(t) \approx -\omega_y^2 \tilde{S}_y(t) e^{-i\omega_y t}$. Moreover, because $\tilde{S}_y(t)$ is slowly varying, further approximations can be made

$$\tilde{S}_y(\alpha_{x,v} t) e^{-i\omega_y \alpha_{x,v} t} \approx \tilde{S}_y(t) e^{-i\omega_y \alpha_{x,v} t} \qquad (3.15)$$

Equation 3.13, under the slow-mover and narrow-band then becomes

$$\psi_{scatt}(y,z,t) = -\iint \frac{\omega_y^2 e^{i\varphi_{x,v}} e^{-i\omega_y \alpha_{x,v} t}}{(4\pi)^2 R_{x,z}(0) R_{x,y}(0)} \times \tilde{S}_y\left(t + T_y - (R_{x,z}(0) + R_{x,y}(0))/c\right) \rho_v(x) d^3v d^3x \tag{3.16}$$

where

$$\varphi_{x,v} \equiv \omega_y^2 \left[R_{x,y}(0) - cT_y + \alpha_{x,v} R_{x,z}(0) \right] / c \tag{3.17}$$

3. Slow-Mover, Narrow-Band and Far-Field Approximation

When the transmitter-to-target and target-to-receiver distances are large in comparison with the scene dimensions, then $|x + vt|$ and $|x + vt|^2 \times \omega_{\max} / c$ can be assumed to be much less than either $|z|$ or $|y|$. And the expansion

$$R_{x,z}(t) = |z - (x - vt)| = |z| - \hat{z} \bullet (x + vt) + \ldots$$

can be applied and similarly for $R_{x,y}(t)$. Substituting the expansions into previous approximations Equation (3.16) then yields

$$\psi_{scatt}(y,z,t) \approx \frac{-\omega_y^2}{(4\pi)^2 |z||y|} \iint e^{i\varphi_{x,v}} e^{-i\omega_y \alpha_{x,v} t} \times \tilde{S}_y\left(t + T_y - (|z| - \hat{z} \bullet \boldsymbol{x} + |y| - \hat{y} \bullet \boldsymbol{x})/c\right) \rho_v(x) d^3v d^3x \tag{3.18}$$

where now

$$\varphi_{x,v} \equiv \omega_y \left[|y| - \hat{y} \bullet \boldsymbol{x} - cT_y + \alpha_v (|z| - \hat{z} \bullet \boldsymbol{x}) \right] / c \tag{3.19}$$

Note that in Equation 3.16, the expansions for $R_{x,z}(t)$, $R_{x,y}(t)$ are used differently. In the amplitude factor, the approximation $R_{x,z}(t) = |z - (x + vt)| \approx |z|$ holds since $|z| \gg |\hat{z} \bullet (x + vt)|$; in the phase factor, however, the product $(\hat{z} \bullet \boldsymbol{x} \times \omega_{\max} / c)$ can still be a

large fraction of 2π, and must be retained. In addition, the signal envelope $\tilde{S}$ can still vary significantly over $|z| - \hat{z}\bullet\boldsymbol{x}$ despite being slowly varying, hence the first order term is retained.

The Doppler scale factor also reduces to

$$\alpha_{\upsilon} \approx \frac{1-\hat{y}\bullet\boldsymbol{v}/c}{1+\hat{z}\bullet\boldsymbol{v}/c} \approx 1-(\hat{y}+\hat{z})\bullet\boldsymbol{v}/c \tag{3.20}$$

where the binomial expansion is used since $|\boldsymbol{v}|/c \ll 1$. The quantity $\omega_y \times \beta_v$ is the Doppler shift (where $\beta_v \equiv -(\hat{y}+\hat{z})\bullet\boldsymbol{v}/c$) and is observed to be dependent on the "bistatic" vector $(\hat{y}+\hat{z})$.

Inserting $T_y = |y|/c$ and setting $k_y \equiv \omega_y / c$

$$\varphi_{x,v} \equiv k_y |\boldsymbol{z}| - k_y(\hat{y}+\hat{z})\bullet\left[\boldsymbol{x} + (\hat{z}\bullet(\boldsymbol{z}-\boldsymbol{x}))\boldsymbol{v}/c\right] \tag{3.21}$$

E. IMAGING VIA A FILTERED ADJOINT

In developing the correlation receiver, it was observed that the "fit" between two complex-valued functions is given by the cross correlation. For correlation reception, the correlation integral seeks out the component of received signal that "matches" the time-delayed, frequency-shifted version of the transmitted signal. Large values of the correlation integral indicate a strong resemblance, while small values indicate weak resemblance. The values of the time-delay and Doppler shift parameters, which maximized the correlation integral, were also the parameters most likely to represent the target.

Using the same notion, imaging can be achieved by determining the position and velocity parameters that represent the best "fit" to the measured data. These will also be the parameters that localize the position and velocity of the unknown scatterers in phase space (position-velocity) space. Cross correlation in the time domain, is multiplication in

the Fourier transform domain (*Fourier correlation theorem*), hence the association with filtering since filters are multiplication operators in the Fourier transform domain.

The model developed for $\psi_{scatt}(y,z,t)$ depends on the position of the scatterer $\boldsymbol{x} = (x_1, x_2, x_3)$ and its velocity $\boldsymbol{v} = (v_1, v_2, v_3)$. Using this form for $\psi_{scatt}(y,z,t)$ to build a six-parameter scattering model based on the arbitrary position $\boldsymbol{p} = (p_1, p_2, p_3)$ and arbitrary velocity $\boldsymbol{u} = (u_1, u_2, u_3)$, the objective will be to determine the values of $\boldsymbol{p}$ and $\boldsymbol{u}$ that maximize the cross correlation between the arbitrary model and the measured data.

In terms of the Doppler shift, the scattered field from known scatterers $\rho_v(x)$ with positions *x* and velocities *v* is

$$\psi_{scatt}(y,z,t) \approx \frac{-\omega_y^2 e^{-i\omega_y(t-|z|/c)}}{(4\pi)^2 \,|\, z \,||\, y \,|} \iint \exp\left\{-ik_y(\hat{y}+\hat{z})\bullet[x - v(t - z\bullet(z-x)/c)]\right\} \times \tilde{S}_y\left(t - (|\, z \,| - (\hat{y}+\hat{z})\bullet x)/c\right)\rho_v(x)d^3v d^3x$$

The effect of data shifted in time is an image that is translated in range. Because this has no bearing on the imaging process, the scattered field result can be simplified by substituting $t' = t - |\, z \,|/c$ which yields

$$\psi_{scatt}(y,z,t') \approx \frac{-\omega_y^2 e^{-i\omega_y t'}}{(4\pi)^2 \,|\, z \,||\, y \,|} \iint \exp\left\{-ik_y(\hat{y}+\hat{z})\bullet[x - v(t' + \hat{z}\bullet x/c)]\right\} \times \tilde{S}_y\left(t' + (\hat{y}+\hat{z})\bullet x/c\right)\rho_v(x)d^3v d^3x \tag{3.22}$$

Ignoring the intensity prefactor, a parametric model representing the field from an unknown point source is

$$\psi(y,z,t') = -e^{-i\omega_y t'} \exp\left\{-ik_y(\hat{y}+\hat{z})\bullet[p - u(t' + \hat{z}\bullet p/c)]\right\} \times \tilde{S}_y\left(t' + (\hat{y}+\hat{z})\bullet p/c\right) \tag{3.23}$$

And the image is created as follows: For each *p* and *u*, determine the function

$$I(p,u) = \iiint \psi_{scatt}(y,z,t')\psi^*(y,z,t')dt'd^m y d^n z \tag{3.24}$$

where *m*, *n* depends on the configuration of the transmitter(s)/receiver(s), and the integrals are over all values of t', *y* and *z* for which measured data is available.

$$I(p,u) = \iiint \psi_{scatt}(y,z,t')\psi^*(y,z,t')Q(\omega,t',p,u,y,z)dt'd^m y d^n z$$

$$\begin{aligned} I(p,u) = -\iiint Q(\omega,t',p,u,y,z) e^{i\omega_y t'} e^{ik_y(\hat{y}+\hat{z})\bullet\left[p-u(t'+\hat{z}\bullet p/c)\right]} \\ \times \tilde{S}_y^*\left(t'+(\hat{y}+\hat{z})\bullet p/c\right)\psi_{scatt}(y,z,t')dt'd^m y d^n z \end{aligned} \tag{3.25}$$

THIS PAGE INTENTIONALLY LEFT BLANK

IV. IMAGING POINT SPREAD FUNCTION

This chapter begins by looking at the radar ambiguity function its relationship to the transmitted waveform, and the accuracy with which target range and velocity can be estimated. The imaging point-spread function (PSF) is also derived based on the new imaging scheme.

A. RADAR AMBIGUITY FUNCTION

For a stationary target, the output of the correlation receiver is the cross correlation between (1) the received signal plus noise and (2) the transmitted signal. In many radar applications, however, the target is moving and so its echo signal has a Doppler frequency shift. The output is therefore a cross correlation between the received signal and the Doppler-shifted transmitted signal.

The nature of the correlation receiver output as a function of both time and Doppler frequency is important for understanding the properties of a radar waveform. In particular, the choice of waveform affects measurement *accuracy*, target *resolution*, and *ambiguities* in range and radial velocity. These aspects of the correlation receiver output will be examined in turn.

When the received echo signal is large compared to noise, the output of the correlation receiver may be written as (see Equations 2.15 and 2.16)

$$\eta(\upsilon,\tau) = \iint_{-\infty}^{\infty} \rho(\upsilon',\tau')\chi(\upsilon-\upsilon',\tau-\tau')e^{i\frac{1}{2}(\upsilon+\upsilon')(\tau-\tau')}d\tau' d\upsilon'$$

where $\chi(\upsilon-\upsilon',\tau-\tau')$ is the radar ambiguity function. The problem of radar imaging is concerned with estimating the location and strength of the point scatterers that are assumed to make up the target. Consequently, understanding χ is essential as the end state involves "inverting" the radar data model. By definition, we have

$$\chi(\upsilon-\upsilon',\tau-\tau') = \int_{-\infty}^{\infty} s_{inc}\left(t'-\frac{1}{2}(\tau-\tau')\right)s_{inc}^{*}\left(t'+\frac{1}{2}(\tau-\tau')\right)e^{i(\upsilon-\upsilon')t'}dt' \qquad (4.1)$$

1. Basic Properties

For simplicity, the origin is chosen to be the true target time-delay and frequency-shift. This assumption will be carried throughout the rest of the discussion. Some key properties that follow from Equation 4.1 [Refs. 14, 18 and 19] are listed

$$\textbf{Signal energy :} \quad \left|\chi(\upsilon,\tau)\right| \le \left|\chi(0,0)\right| \tag{4.2}$$

$$\textbf{Ambiguity volume :} \quad \iint_{-\infty}^{\infty} \left|\chi(\upsilon,\tau)\right|^2 d\tau d\upsilon = 1 \qquad (\textit{normalized signal}) \tag{4.3}$$

$$\textbf{Symmetry :} \quad \left|\chi(-\upsilon,-\tau)\right| = \left|\chi(\upsilon,\tau)\right| \tag{4.4}$$

$$\textbf{Frequency - domain :} \quad \chi(\upsilon,\tau) = \frac{1}{2\pi}\int_{-\infty}^{\infty} s_{inc}(\omega - \frac{1}{2}\upsilon) s_{inc}^{*}(\omega + \frac{1}{2}\upsilon) e^{-i\omega\tau} d\omega \tag{4.5}$$

Equation 4.2 states that the maximum value of the ambiguity function occurs at the origin (true target time-delay and frequency-shift). Equation 4.3 asserts that the total volume under the ambiguity surface is a constant. This gives rise to a *radar uncertainty principle*: choosing a signal $s(t)$ so that the ambiguity surface will be narrow in one dimension will cause it to be correspondingly wide in the other dimension. In the case of range-Doppler imaging, a waveform with good range resolution has poor Doppler resolution and vice versa.

2. Range Resolution

Equation 4.5 presents an intuitive look at range resolution. Consider a fixed target $(\upsilon = 0)$ and rewrite Equation 4.5 as

$$|\chi(0,\tau)| = \frac{1}{2\pi}\left|\int_{-\infty}^{\infty} |s_{inc}(\omega)|^2 e^{-i\omega\tau} d\omega\right| \tag{4.6}$$

Recognize the form of Equation 4.6 as the inverse Fourier transform of the transmitted power spectral density. Then, in order for $|\chi(0,\tau)|$ to have high resolution in τ measurements (ideally a delta function), the power spectral density has to be identically

one; such a signal will be broadly supported in the Fourier domain. Hence, it is clear that better range resolution is obtained when the signal bandwidth is large.

A more rigorous study of estimation errors in the presence of Gaussian noise is developed in [1] by examining the behavior of the ambiguity function in the neighborhood of its main peak. This study shows that estimation error of υ and τ is described by an ellipse, and that time-domain resolution is inversely proportional to frequency-domain bandwidth. Hence, bandwidth is inherently important to problems in radar target imaging. A further interesting result makes uses of the definition of bandwidth in terms of the second moments (probabilistic variance) of the power spectrum for a narrow-band signal $s(t) = a(t)e^{i\Phi(t)}$. We can write

$$\beta^2 = \frac{1}{2}\int_{-\infty}^{\infty}\left|\frac{da(t')}{dt'}\right|^2 dt' + \frac{1}{2}\int_{-\infty}^{\infty}\left(\frac{d\Phi(t')}{dt'}\right)^2 |a(t')|^2\, dt' - \omega_0^2 \tag{4.7}$$

where β represents bandwidth. This useful relationship illustrates that a nonlinear $\Phi(t)$ (phase modulation) will increase the bandwidth in comparison with signals that are modulated in amplitude only. This is the basis for pulse compression (see Chapter V), a technique of practical importance because it allows for the creation of fine range-resolution waveforms that are also of long duration with sufficient energy on target.

3. Doppler Resolution

To study Doppler resolution, consider a target whose range is known. Thus, setting $\tau = 0$ in Equation 4.1 yields

$$|\chi(\upsilon,0)| = \left|\int_{-\infty}^{\infty} |s_{inc}(t')|^2 e^{i\upsilon t'} dt'\right| \tag{4.8}$$

It is evident that better Doppler resolution is obtained from a long duration signal. This is in stark contrast to range resolution requirements. In addition, the Doppler resolution is determined only by the amplitude modulation of the signal and not by the phase.

B. IMAGE ANALYSIS

From Chapter III, an explicit form for the image is

$$I(p,u) = -\iiint Q(\omega,t',p,u,y,z) e^{i\omega_y t'} e^{ik_y(\hat{y}+\hat{z})\bullet\left[p-u(t'+\hat{z}\bullet p/c)\right]} \times \tilde{S}_y^*\left(t'+(\hat{y}+\hat{z})\bullet p/c\right)\psi_{scatt}(y,z,t')dt'd^m y d^n z \tag{4.9}$$

To examine the performance of the imaging scheme, the ideal (expected) data are inserted back into the image equation. Substituting for $\psi_{scatt}(y,z,t')$ yields

$$I(p,u) = \iiint\iint \frac{\omega_y^2 Q(\omega,t',p,u,y,z)}{(4\pi)^2 |z||y|}\rho_v(x) \times \exp\left\{ik_y(\hat{y}+\hat{z})\bullet[p-x-(u-v)t'-u(\hat{z}\bullet p)/c+v(\hat{z}\bullet x)/c]\right\} \times \tilde{S}_y^*\left(t'+(\hat{y}+\hat{z})\bullet p/c\right)\tilde{s}_y\left(t'+(\hat{y}+\hat{z})\bullet x/c\right)d^3v d^3x dt' d^m y d^n z \tag{4.10}$$

The distances $|z|$ and $|y|$ are scaling amplitude factors and not essential for imaging purposes. Thus, choose

$$Q(\omega,t',p,u,y,z) = \frac{(4\pi)^2 |z||y|}{\omega_y^2} J(p,u,y,z) \tag{4.11}$$

where $J(p,u,y,z)$ depends on the geometry and is chosen to compensate for a Jacobian that results from the integral of the variable *t'*

$$I(p,u) = \iiint\iint \tilde{S}_y^*\left(t'+(\hat{y}+\hat{z})\bullet p/c\right)\tilde{S}_y\left(t'+(\hat{y}+\hat{z})\bullet x/c\right)e^{-ik_y(y+z)\bullet(u-v)t'} \times \exp\left\{ik_y(\hat{y}+\hat{z})\bullet[p-x-u(\hat{z}\bullet p)/c+v(\hat{z}\bullet x)/c]\right\} \times J(p,u,y,z)\rho_v(x)dt'd^3v d^3x d^m y d^n z \tag{4.12}$$

Equation 4.12 can be written as

$$I(p,u) = \iint K(p,u,y,z)\rho_v(x)d^3v d^3x \tag{4.13}$$

where

$$K(p,u,y,z)=\iint \exp\left\{-ik_y(\hat{y}+\hat{z})\bullet[u(\hat{z}\bullet p)-v(\hat{z}\bullet x)]/c\right\}$$
$$\times\int \tilde{S}_y^{*}\left(t'+(\hat{y}+\hat{z})\bullet p/c\right)\tilde{S}_y\left(t'+(\hat{y}+\hat{z})\bullet x/c\right)e^{-ik_y(\hat{y}+\hat{z})\bullet(u-v)t'}dt' \qquad (4.13)$$
$$\times J(p,u,y,z)d^m y d^n z$$

is the point-spread function describing the behavior of the imaging system. Equation 4.12 caters for multiple transmitters and receivers where *y* and *z* represent the transmitter and receiver location respectively. The corresponding superscript *m* and *n* accounts for the total number of transmitter and receivers. Apply the change of variables $t=t'+\frac{1}{2}(\hat{y}+\hat{z})\bullet(p+x)/c$ and set $\tau\equiv(\hat{y}+\hat{z})\bullet(p-x)/c$ to obtain

$$K(p,u,y,z)=\iint \exp\left\{-ik_y(\hat{y}+\hat{z})\bullet[u(\hat{z}\bullet p)-v(\hat{z}\bullet x)]/c\right\}$$
$$\times\exp\left\{ik_y(\hat{y}+\hat{z})\bullet[(p-x)+\frac{1}{2}(u-v)(\hat{y}+\hat{z})\bullet(p+x)]/c\right\} \qquad (4.14)$$
$$\times\left[\int_{-\infty}^{\infty}\tilde{S}_y^{*}\left(t+\frac{1}{2}\tau\right)\tilde{S}_y\left(t-\frac{1}{2}\tau\right)e^{-ik_y(\hat{y}+\hat{z})\bullet(u-v)t}dt\right]J(p,u,y,z)d^m y d^n z$$

The integral in square brackets is the radar ambiguity function

$$\chi(\upsilon,\tau)=\int_{-\infty}^{\infty}\tilde{S}_y^{*}\left(t+\frac{1}{2}\tau\right)\tilde{S}_y\left(t-\frac{1}{2}\tau\right)e^{-i\upsilon t}dt$$

χ is determined by the transmitted signal and $|\chi|$ attains its maximum value at $p=x$, $u=v$ for general configurations of transmitters/receivers. So the imaging PSF can be written as

$$K(p,u,y,z)=\iint \exp\left\{-ik_y(\hat{y}+\hat{z})\bullet[u(\hat{y}\bullet p)-v(\hat{z}\bullet x)]/c\right\}$$
$$\times\exp\left\{ik_y(\hat{y}+\hat{z})\bullet[(p-x)+\frac{1}{2}(u-v)(\hat{y}+\hat{z})\bullet(p+x)]/c\right\} \qquad (4.15)$$
$$\times\chi\left(k_y(\hat{y}+\hat{z})\bullet(u-v),(\hat{y}+\hat{z})\bullet(p-x)/c\right)J(p,u,y,z)d^m y d^n z$$

THIS PAGE INTENTIONALLY LEFT BLANK

V. PULSE COMPRESSION

Detection of signals in noise and resolving capability are both fundamental to radar imaging. As discussed in Chapter II and IV, the use of correlation reception and a transmitted waveform with nonlinear phase modulation provides means to enhance performance in detection and resolution. Pulse compression is a technique that fuses these concepts and involves transmitting long coded pulses, together with signal processing methods such as correlation reception. This is of practical importance because it allows for the creation of fine range-resolution waveforms that are also of long duration. This increases radiation energy directed on target without relying solely on boosting radar transmitted power. This chapter gives a physical interpretation of pulse compression and looks at a specific phase-coded signal known as the *chirp*.

A. REVISITING CORRELATION RECEPTION

Recall that in Chapter II we showed that the output of the correlation receiver is a correlation integral between the received signal and a time-delayed, Doppler-shifted version of the transmitted signal. It is illustrative to explain the phenomenon of pulse compression with a graphical example. Using the simple one-dimensional imaging case in Equation 2.12, the correlation receiver output can be written as

$$\eta(t) = \int_{-\infty}^{\infty} s^*(t') s_{rec}(t'+t)\,dt' \tag{5.1}$$

which is a *correlation* between *s* and s_{rec}. If $s = s_{rec}$ (reflectivity function is 1), Equation 5.1 is called an *autocorrelation*. In Figure 5, the signal at the top represents the transmitted waveform. The lower graphs represent the received signal for different shifts, according to Equation 5.1. When a signal shifted by *t* is multiplied by the waveform at the top and the product is integrated over *t'*, the resulting number is plotted at position *t* on the graph to the right.

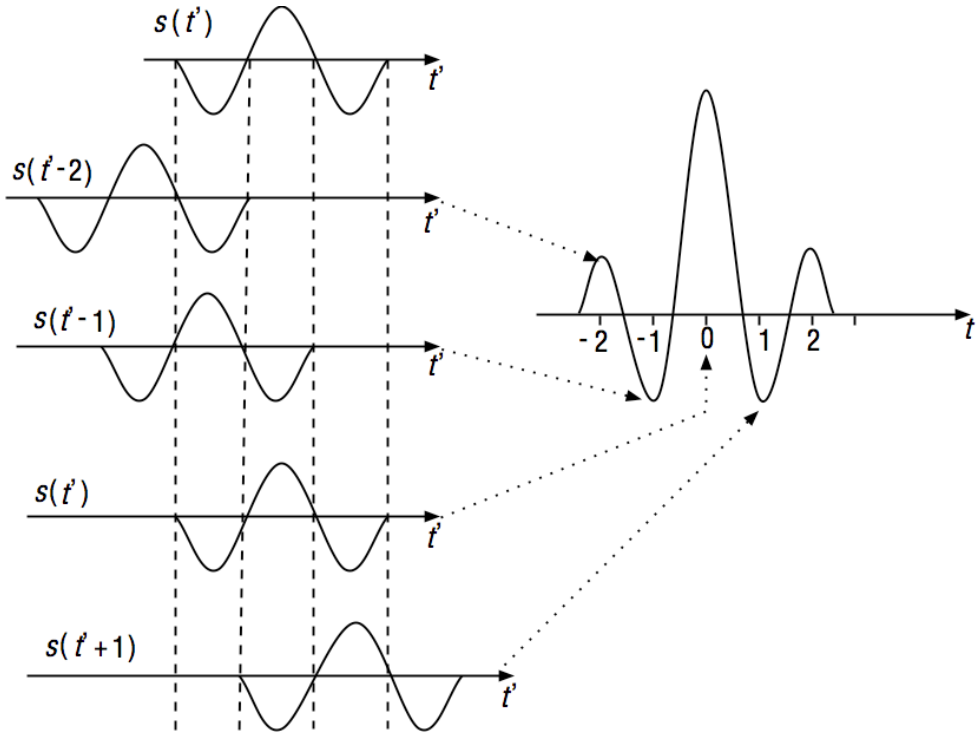

Figure 5. Phenomenon of pulse compression where the energy is concentrated at a single delay time. From [18].

Figure 5 shows that although the output signal has a longer time duration than the original signal *s*, its energy is more concentrated at a single delay time. It is a consequence of the Cauchy-Schwarz inequality that the highest peak occurs when the signals are not shifted relative to each other. The smaller peaks, called sidelobes, are undesirable and an open problem is to design pulses whose autocorrelations have the lowest and fewest sidelobes.

B. PHASE CODING—CHIRPS

A radar system makes the most efficient use of power when it transmits a constant-amplitude waveform. Consequently, most radar waveforms are designed with variations only in the phase of the signal. The most important and most commonly-used radar waveform is the *chirp*. A chirp is a constant-amplitude signal whose instantaneous frequency varies linearly with time; chirps are therefore also called *Linearly Frequency*

Modulated (LFM) waveforms. Linear variation of the instantaneous frequency implies that $d\phi / dt = \omega_{\min} + \gamma t$. The coefficient γ is called the angular *chirp rate*. A chirp is thus of the form

$$s(t) = e^{i(\omega_{\min} t + \frac{1}{2}\gamma t^2)} u_{[0,T]}(t) \tag{5.2}$$

where $u_{[0,T]}(t)$ is 1 in the interval [0, *T*] and 0 otherwise.

A chirp with positive chirp slope is called an upchirp; one with a negative chirp slope is a downchirp. The instantaneous (angular) frequency of the chirp varies from $\omega_{\min}$ to $\omega_{\max} = \omega_{\min} + \gamma t$, with a center frequency of $\omega_0 = \omega_{\min} + \gamma t / 2$. Thus, the instantaneous frequency of the chirp varies over the interval $\left[\omega_0 - T\gamma / 2, \omega_0 + T\gamma / 2\right]$. The power spectrum of a chirp is roughly constant over the frequency band $\left[\omega_0 - T\gamma / 2, \omega_0 + T\gamma / 2\right]$, thus the angular frequency bandwidth $T\gamma$ can be estimated by looking at the range of instantaneous frequencies (see Figure 6).

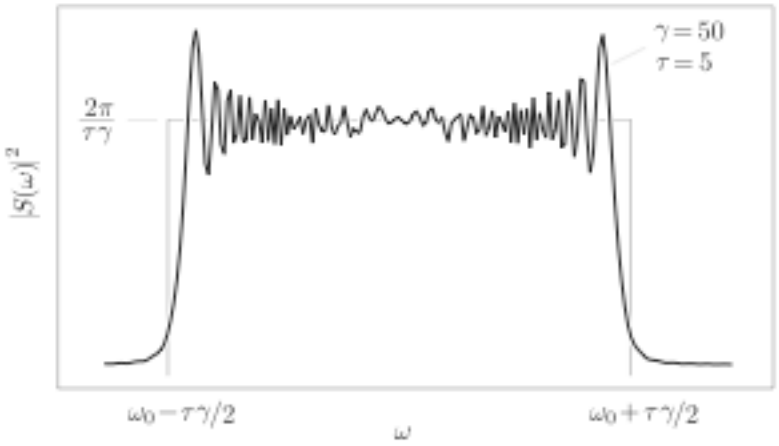

Figure 6. Spectrum for a chirp pulse of length τ. From [1].

Chirps are very commonly used in radar imaging. Pulse compression for chirps has the following intuitive interpretation: When the pulse is transmitted, different parts of

the pulse are coded with different instantaneous frequencies. In the pulse compression process, the different frequencies are delayed by different amounts of time, so that all the energy emerges at the same time [18].

C. AMBIGUITY FUNCTION FOR COMMON WAVEFORMS

From the preceding discussion, the "ideal" ambiguity function will typically consist of a single peak of infinitesimal thickness at the origin and be zero everywhere else. It will closely approximate an impulse function, and have no ambiguities in range or Doppler frequency shift. The infinitesimal thickness at the origin will permit the time delay and/or frequency shift to be determined simultaneously to as high a degree of accuracy as desired. Such a highly desirable ambiguity function, however, is not theoretically allowed. The properties of the ambiguity function implicitly mandate that trade-offs exist between the measured dimensions.

In practice, other than the trade-offs in dimension resolution, waveforms also generally have significant responses outside the narrow region in the near vicinity of the origin, i.e. there are many possible ambiguous (blind) range and Doppler. Ambiguities are a consequence of discontinuous waveforms, such as in a pulse train. The resolution for single rectangular pulse, single chirp and coherent pulse trains will be discussed next.

1. Resolution for a Single Rectangular Pulse

Time domain impulses have infinite bandwidth; hence they are idealized signals. More realistic waveforms can be modeled, for example, as

$$s_{inc}(t) = \begin{cases} 1 & \text{if } 0 < t \le T, \\ 0 & \text{otherwise.} \end{cases} \tag{5.3}$$

for which $s_{inc}(t - 1/2\tau)s^*_{inc}(t + 1/2\tau)$ is non-zero in the interval $t \in (|\tau|/2,\ T - |\tau|/2)$. The ambiguity function is then

$$\chi(\upsilon,\tau) = \int_{-\infty}^{\infty} s_{inc}(t' - \frac{1}{2}\tau) s_{inc}^{*}(t' + \frac{1}{2}\tau) e^{i\upsilon t'} dt' = \int_{|\tau|/2}^{T-|\tau|/2} e^{i\upsilon t'} dt'$$

$$= \frac{1}{i\upsilon} e^{i\upsilon(T/2)} \left[e^{i\upsilon(T/2-|\tau|/2)} - e^{-i\upsilon(T/2-|\tau|/2)} \right] \tag{5.4}$$

$$= (T - |\tau|) e^{i\upsilon T/2} \mathrm{sinc}\left[\frac{1}{2}\upsilon(T - |\tau|) \right]$$

For $\upsilon = 0$, then the delay resolution (by the peak-to-first-null measure) as observed from the ambiguity surface $|\chi(0,\tau)|^2$, is $\Delta\tau = T$ (zero-crossing at $\tau = T$), which corresponds to a range resolution of $\Delta R = cT/2$. For $\tau = 0$, the ambiguity surface $|\chi(\upsilon,0)|^2$ yields $\Delta\upsilon = 1/T$ because the first zero of the *sinc* function occurs when its argument is π. The Doppler shift is related to down-range relative velocity by $\upsilon_D = -2v\upsilon_0 / c$ (see Equation 2.4), and the corresponding velocity resolution is $\Delta v = \lambda_0 / 2T$.

2. Resolution for a Single Chirp

A chirped signal provides another example of a ridge-type ambiguity function produced by linearly frequency modulating a rectangular pulse over a bandwidth β. The pulse width T is large compared to $1/\beta$. The frequency modulation increases the spectral bandwidth of the pulse so that $\beta T \gg 1$. Because the pulse width T and the bandwidth β can be chosen independent of one another, the time-delay and frequency accuracies are independent of the other.

The *chirp* signal is one whose frequency changes linearly with time

$$s_{inc}(t) = \begin{cases} \exp\left(-i\frac{1}{2}\gamma t^2 \right) & \text{if } 0 < t \le T, \\ 0 & \text{otherwise.} \end{cases} \tag{5.5}$$

The constant γ is known as the *chirp rate*. The ambiguity function is then

$$\chi(\upsilon,\tau) = \int_{-\infty}^{\infty} s_{inc}(t'-\frac{1}{2}\tau)s_{inc}^{*}(t'+\frac{1}{2}\tau)e^{i\upsilon t'}dt' = \int_{|\tau|/2}^{T-|\tau|/2} e^{i(\upsilon+\gamma\tau)t'}dt'$$

$$= \frac{1}{i(\upsilon+\gamma\tau)} e^{i(\upsilon+\gamma\tau)T/2}\left[e^{i(\upsilon+\gamma\tau)(T/2-|\tau|/2)} - e^{-i(\upsilon+\gamma\tau)(T/2-|\tau|/2)} \right] \tag{5.6}$$

$$= (T-|\tau|)e^{i(\upsilon+\gamma\tau)T/2}\text{sinc}\left[\frac{1}{2}(\upsilon+\gamma\tau)(T-|\tau|)\right]$$

Observe that a chirp leads to an ambiguity function that is a *sinc*-function in both the time and frequency domain. It is instructive to examine this property again by looking at the signal resolution.

For $\tau = 0$, a similar result of $\Delta\upsilon = 1/T$ is obtained as in the case of the rectangular pulse. This is because the amplitude modulation is identical in both cases. Consequently, Doppler resolution is the same. However, with phase modulation, it is expected that the delay resolution, and therefore resolution will be enhanced.

For $\upsilon = 0$, when $\tau > 0$ the first null occurs when $\pi = (T-\tau)\gamma\tau/2$. Reference [19] shows that the expression $\pi = (T-\tau)\gamma\tau/2$ has a quadratic equation form with a solution $\Delta\tau = 2\pi/\gamma T$, which corresponds to a range resolution of $\Delta R = c/\beta$ where $\beta = 2\pi\gamma T$ is the bandwidth in Hertz. For $\tau = 0$, $\Delta\upsilon = |\chi(\upsilon,0)|^2 = 1/T$ because the first zero of the *sinc* function occurs when its argument is π. The Doppler shift is related to down-range relative velocity by $\upsilon_D = -2v\upsilon_0/c$ (see Equation 2.4), and the corresponding velocity resolution $\Delta v = \lambda_0/2T$.

The pulse compression ratio is defined as the product of pulse spectral bandwidth β and the uncompressed pulsewidth *T*. Comparing the range resolution between the single rectangular pulse and single chirp,

$$\frac{\Delta R_{\text{rectangular}}}{\Delta R_{\text{chirp}}} = \frac{cT/2}{c/\beta} = \frac{\beta T}{2} \tag{5.7}$$

In other words, phase modulation improves the range resolution by a factor of one half the time-bandwidth product.

3. Resolution for Coherent Pulse Trains

Following the analysis given in [18], a train of *N* identical pulses is considered:

$$s(t) = \frac{1}{\sqrt{N}} \sum_{n=0}^{N-1} u(t - nT_R) \tag{5.8}$$

where T_R is the pulse repetition interval, which might be on the order of 1ms. The reciprocal $1/T_R$ is called the pulse repetition frequency (PRF).

The ambiguity function for the pulse train is

$$\begin{aligned} \chi(\upsilon,\tau) &= \frac{1}{N} \sum_{n=0}^{N-1} \sum_{m=0}^{N-1} \int u^*(\tau + \tau' - mT_R) u(\tau' - nT_R) e^{i\upsilon\tau'} d\tau' \\ &= \frac{1}{N} \sum_{n=0}^{N-1} \sum_{m=0}^{N-1} \chi_u\left(\tau - (n-m)T_R, \upsilon\right) e^{i\upsilon n T_R} \end{aligned} \tag{5.9}$$

where χ_u denotes the ambiguity function for *u* and where we have used the substitution $t'' = \tau' - nT_R$. A lengthy calculation involving rearrangement of the order of summation and the summing of a geometric series results in

$$\chi(\upsilon,\tau) = \frac{1}{N} \sum_{p=-(N-1)}^{N-1} \chi_u(\tau - pT_R, \upsilon) e^{i\upsilon T_R (N-1-|p|)} \frac{\sin\left[\pi\upsilon T_R (N - |p|)\right]}{\sin(\pi\upsilon T_R)} \tag{5.10}$$

If the pulses *u* are sufficiently well-separated so their ambiguity functions χ_u do not overlap, then we take the absolute value of Equation 5.13 to obtain

$$|\chi(\upsilon,\tau)| = \frac{1}{N} \sum_{p=-(N-1)}^{N-1} |\chi_u(\tau - pT_R, \upsilon)| \left| \frac{\sin\left[\pi\upsilon T_R (N - |p|)\right]}{\sin(\pi\upsilon T_R)} \right| \tag{5.11}$$

Such an ambiguity function has a “bed of nails” appearance (see Figure 7), with peaks at $\tau = pT_R$, $p = -(N-1), -(N-2), ..., 0, 1, ..., (N-1)$ and υ such that $\pi\upsilon T_R N = (m + 1/2)\pi$, $m = 0, 1, 2, ...$

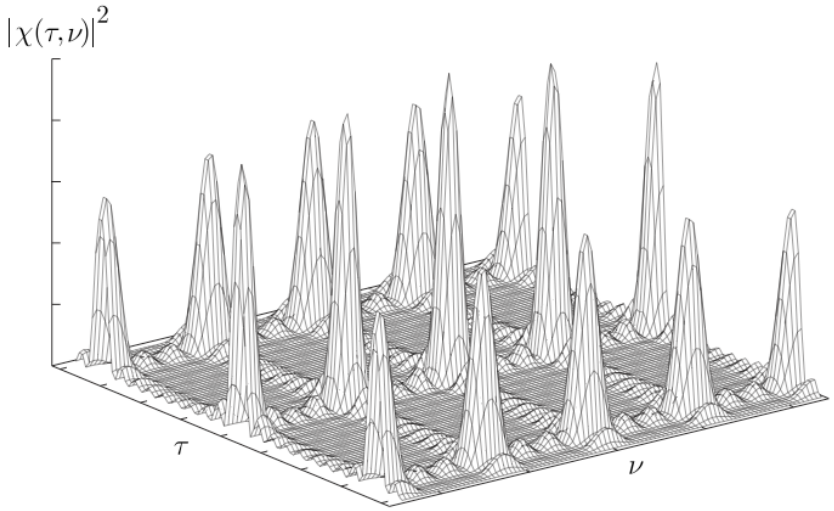

Figure 7. Ambiguity Function for a train of pulses. From [2]

Following the previous analysis, consider the $\upsilon = 0$ cut of the ambiguity surface to estimate the range resolution yields

$$|\chi(0,\tau)| = \frac{1}{N}\sum_{p=-(N-1)}^{N-1} |\chi_u(\tau - pT_R, 0)|(N - |p|) \tag{5.12}$$

where we have used the fact that $\lim_{x\to 0}[\sin bx]/\sin x = b$. We see that the range resolution of the main peak is the same as the range resolution of the individual pulse *u*, but that we now have range ambiguities due to the extraneous peaks at $\tau = pT_R$.

To estimate the Doppler resolution, consider the $\tau = 0$ cut of Equation 5.11 and for well-separated pulses, only the *p=0* term contributes

$$|\chi(\upsilon,0)| = \frac{1}{N}\sum_{p=-(N-1)}^{N-1} |\chi_u(0,\upsilon)| \left|\frac{\sin[\upsilon T_R N]}{\sin[\upsilon T_R]}\right| \tag{5.13}$$

Consider the numerator argument because it varies much faster. It shows that the Doppler resolution is $1/NT_R$, and hence the Doppler resolution of the pulse train is higher than that of a single pulse.

The many ambiguities produced by a pulse train may appear to lead to a poor radar waveform. The time-delay measurement accuracy, determined by pulsewidth *T* and the frequency accuracy (determined by the pulse repetition interval T_R) can be selected independently. If pulse repetition interval T_R is such that no radar echoes are expected with a time delay greater than T_R, and no Doppler-frequency shifts are expected greater than $1/T_R$, then the effective ambiguity function reduces to just a single spike at the origin whose dimensions are determined by *T* and T_R. In practice, ambiguities can also be resolved with different PRF, and many radars employ this type of waveform.

THIS PAGE INTENTIONALLY LEFT BLANK

VI. RESULTS AND CONCLUSION

This chapter shows how the new imaging algorithm (Equation 3.25) is implemented and analyzed. Recall from Chapter III that the image is formed when the correlation receiver observed a "fit" between the scattering model (Equation 3.22) and the parametric radar model (Equation 3.23). For correlation reception, the correlation integral seeks out the component of the received signal that "matches" the time-delayed, frequency-shifted version of the transmitted signal. Large values of the correlation integral indicate a strong resemblance while small values indicate a weak resemblance. The values of the time-delay and Doppler shift parameters that maximized the correlation integral were also the parameters most likely to represent the target. Using the same notion, three sets of Matlab programs were used for the implementation:

1. The Scattering model (Equation 3.22)

Scattering Model $\psi_{scatt}(y,z,t)$ is basically the measured data from the scatterer. It provides all the information of the scatterer position $\boldsymbol{x} = (x_1, x_2, x_3)$ and velocity $\boldsymbol{v} = (v_1, v_2, v_3)$. A code is built (refer to Appendix) numerically based on a six-parameter scattering model and capable for different types of waveforms.

2. The Radar Model (Equation 3.23)

Using the same form as the scattering model, a similar set of code is built (refer to Appendix) numerically based on arbitrary position $\boldsymbol{p} = (p_1, p_2, p_3)$ and arbitrary velocity $\boldsymbol{u} = (u_1, u_2, u_3)$. The objective will be to determine the values of $\boldsymbol{p}$ and $\boldsymbol{u}$ that maximize the cross correlation between the arbitrary model and the measured data.

3. The Image Model (Equation 3.24)

The image model forms the main routine of the code (refer to Appendix). It calls the parametric radar model as a sub-routine and cross correlated it to the scattering model.

As part of the development effort to build the full scale imaging algorithm, this thesis will focus on imaging a single static point scatterer. The result of the image is also used for comparison with the point spread function image. Equation 3.24 does not restrict the choice of transmitted waveform nor the transmitter/receiver configuration. The objective here is to study the behavior of the new imaging scheme with a single pulse waveform and under different transmitter/receiver configuration.

Figure 8 shows the transmitter/receiver geometries for the simulation performed. The receivers are denoted by "Δ" while the transmitter is denoted by "$+$". Figure 8(a) and (b) are used to show the straight line receiver configuration while Figure 8(c) shows the circular receiver configuration.

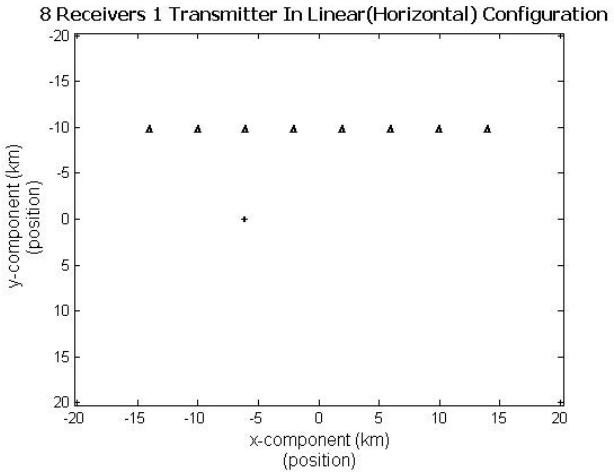

(a)

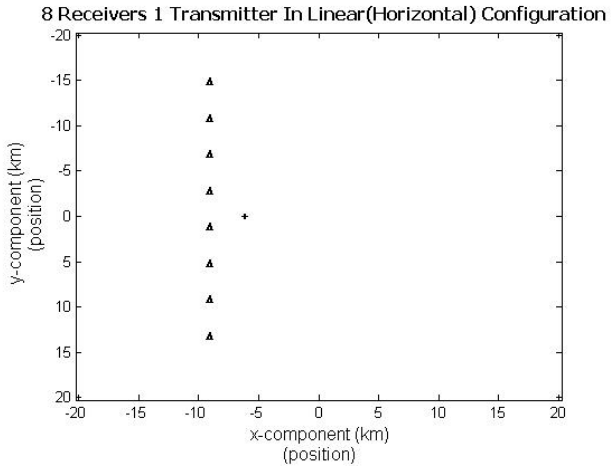

(b)

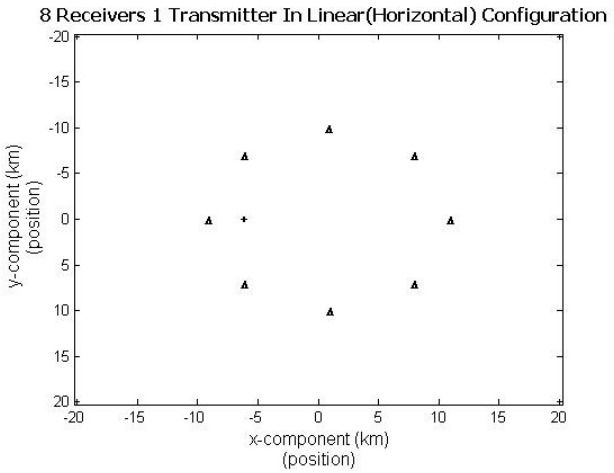

(c)

Figure 8. Transmitter/Receiver configurations

A. IMAGING A STATIC POINT TARGET FOR SINGLE RECTANGULAR PULSE

The transmitted waveform used is a single rectangular pulse defined in Equation 5.6. This waveform is substituted into Equation 3.24 and implemented in Matlab. Equation 3.24 is capable of determining a three-dimensional distribution of position in space and the corresponding three-dimensional velocities (i.e. a six-dimensional phase space image). However, to study the effects of transmitter/receiver geometry and translation in position on the imaging scheme, the use of two-dimensional plots of the target image in position space will suffice.

1. Localization of Point-Scatterer in Position Space

The point target or scatterer is located at position $(x_1, x_2) = (0,0)$. Two dimensional plots of the target image in position space for 4, 9, 36 and 180 receivers are given in Figures 9(a)–(d) respectively. It is shown that the point scatterers are localized in position space about the scatterer position (0,0). However, under the different geometries,

the point scatterer is represented differently; this is shown in Figure 10(a)–(d) and 11(a)–(d); it can be observed that the geometry of the transmitters/receivers plays an important role in shaping the target image.

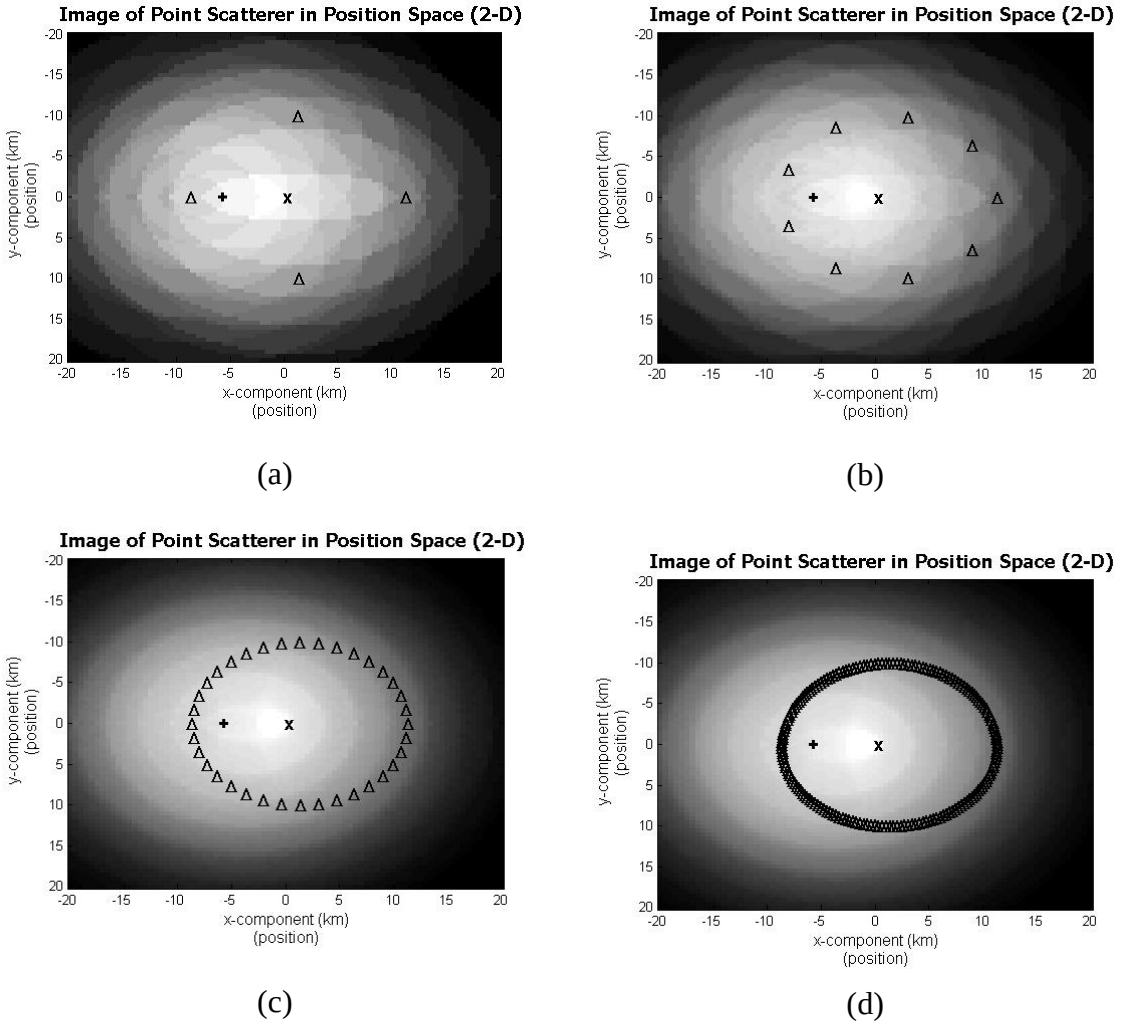

Figure 9. 2-D Localization of point-scatterer in position space (for rectangular pulse).

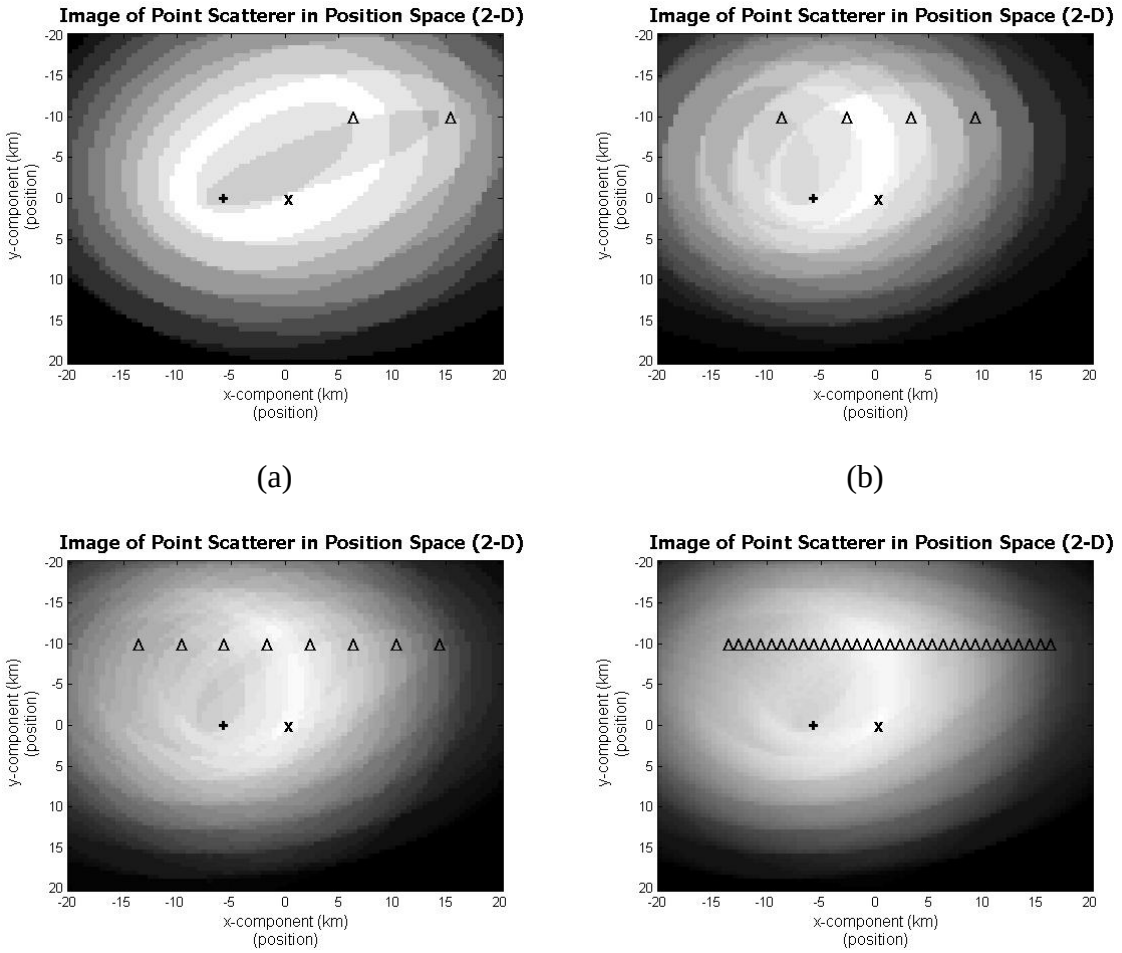

Figure 10. Transmitter/Receiver in linear (horizontal) configurations

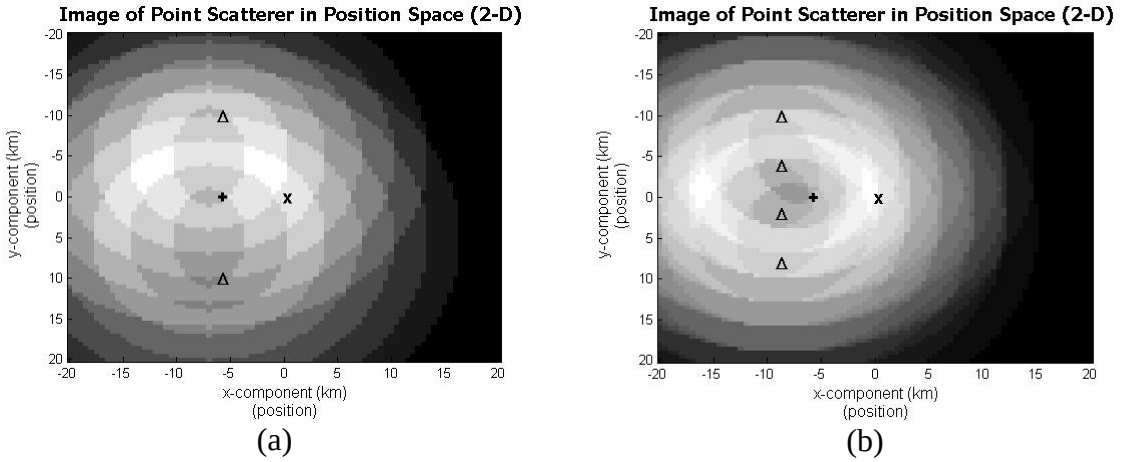

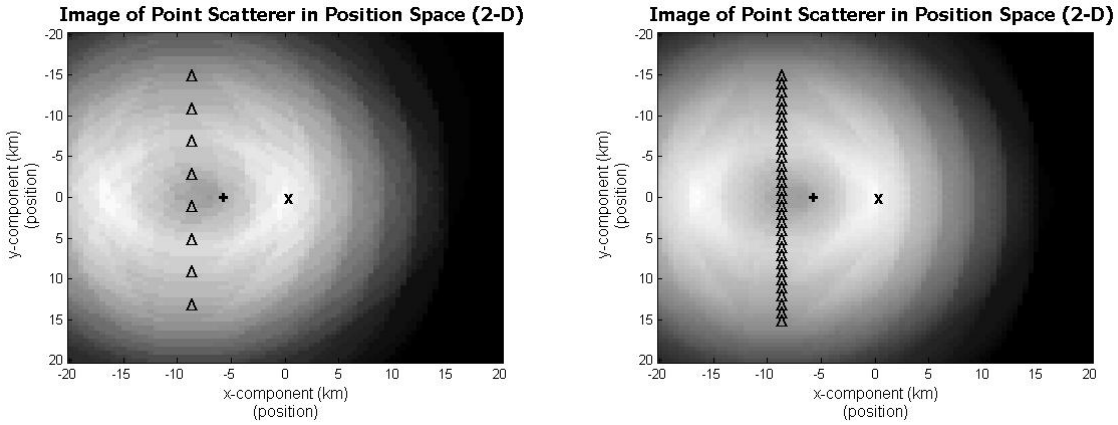

(c) (d)

Figure 11. Transmitter/Receiver in linear (vertical) configurations

2. Comparison with PSF Image

When compared with a PSF image, both the images show that the point scatterer localized in position space; however it is observed that the PSF gives a smoother spread compared to the imaging code. This could be due to the fact that the PSF code is built based on an analytical approach where as the imaging code is built based on the numerical approach, and as a result there will be some round off errors.

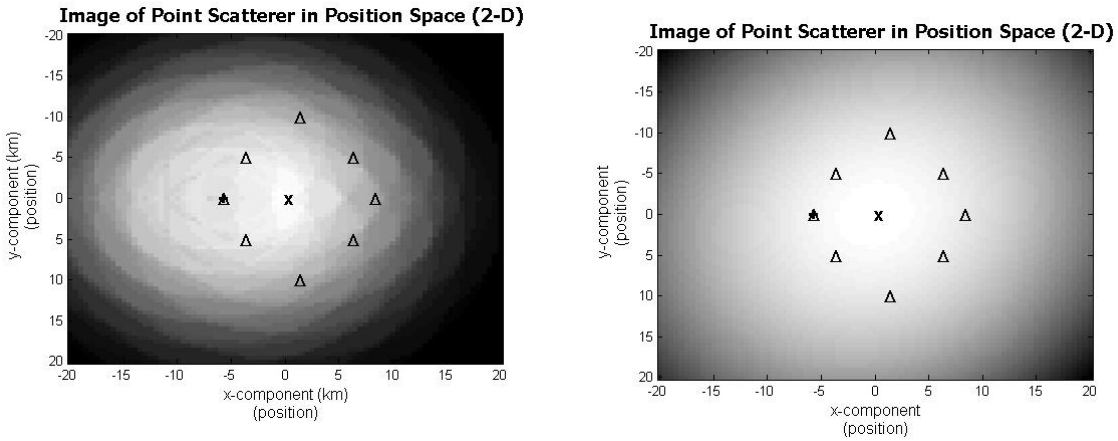

(a) (b)

Figure 12. Comparison with PSF (target at $(x_1, x_2) = (0,0)$)

B. CONCLUSIONS

Image artifacts result when motion in the imaging scene is not addressed. In recent years, a number of attempts to develop imaging techniques that can handle moving objects have been proposed. However, all of these techniques rely on making the approximation that a target in motion is assumed to be momentarily stationary while it is being interrogated by a radar pulse. This thesis is a study of the new imaging approach developed by *Cheney* and *Borden* [2] that can accommodate target motion during the imaging process.

In this thesis, the subject of radar imaging from scattered waves is explored and applied to the new imaging approach. The simulation result using Matlab obtained showed that the new imaging scheme is well behaved; specifically, it localizes the target in space and is translation invariant. In addition, it is apparent that the geometry of the transmitters and receivers disposition affects the behavior of the imaging system.

This work represents the early stages of development of a full imaging algorithm applicable to moving targets in a multistatic environment. Follow-on work will include further simulation efforts. This thesis used single pulse radar waveforms and a single transmitter, but in reality, fielded radar systems typically utilize pulse compression techniques and send out long, coded pulse trains. Neither need the multistatic radar system be restricted to one transmitter. In this case, the imaging scheme has to be adjusted to incorporate more realistic radar waveforms and optimize the transmitter/receiver geometries for implementing the imaging algorithm. These will be used to support the development of the eventual imaging algorithm. Finally, real world target data can then be applied to the developed imaging algorithm to assess its performance.

THIS PAGE INTENTIONALLY LEFT BLANK

APPENDIX: MATLAB CODES

IMAGING CODE

```
%%%%%%%%%%%%%%%%%%%%%%%%%%%%%%%%%%%%%%%%%%%%%%%%%%%%%%%%%%%%%%%%%%%%%%%%
%% This Program evaluates the Image of a single point target

% The program uses the approach, techniques on imaging from Professor Borden, Brett
% The Waveform adopted is a 1 x 11 Rect Signal.
% The Program load the sample_data.mat from the Make_Data.m and correlate it to radar model in predict.m subroutine.
%%%%%%%%%%%%%%%%%%%%%%%%%%%%%%%%%%%%%%%%%%%%%%%%%%%%%%%%%%%%%%%%%%%%%%%%
clear

load sample_data.mat Rx Ry Tx Ty w k_y T delta_T D N

N=length(Rx);
NN=length(Tx);

J=1; %Set Jacobian to 1

% Define the area of the Scene (10km by 10km)
p_x_start=-20;
p_x_end=20;
p_y_start=-20;
p_y_end=20;

res_p=0.5; %Nyquist Sampling rate.
p_x=p_x_start:res_p:p_x_end;
p_y=p_y_start:res_p:p_y_end;
nx=length(p_x);
ny=length(p_y);

I=zeros(nx,ny);

for py=1:ny
for px=1:nx
P=10^3*[p_x_start+((py-1)*res_p);p_y_end-((px-1)*res_p)];
expect=predict(P,Rx,Ry,Tx,Ty,N,NN,w,k_y,T,delta_T);
for n=1:N
I(px,py)=I(px,py)+D(n,:)*expect(n,:)'*J;
end
end
end
```

```
%% Output Plot
colormap(gray)
imagesc(p_x,p_y,flipud(abs(I)))
%colorbar
xlabel({'\fontsize{12}   x-component   (km)','\fontsize{12}
(position)'})
ylabel({'\fontsize{12}   y-component   (km)','\fontsize{12}
(position)'})
title('\bf \fontsize{14} \fontname{tahoma} Image of Point
Scatterer in Position Space (2-D)')
text(Tx(1)/10^3,Ty(1)/10^3,'\bf \fontsize{14} +')

for i=1:N
text(Rx(i)/10^3,Ry(i)/10^3,'\bf \fontsize{9} \Delta')
end
```

SAMPLE DATA MODEL CODE

```
%%%%%%%%%%%%%%%%%%%%%%%%%%%%%%%%%%%%%%%%%%%%%%%%%%%%%%%%%%%%%%%%%%%%%%%%
%% This Program Create sample data set
% The program uses the approach, techniques on imaging from
Professor Borden, Brett
%%%%%%%%%%%%%%%%%%%%%%%%%%%%%%%%%%%%%%%%%%%%%%%%%%%%%%%%%%%%%%%%%%%%%%%%

%circular receiver configuration
r=10;
a=0:1.5:360;
b=a*pi/180;
N=241;
Rx=10^3*r*cos(b);
Ry=10^3*r*sin(b);

% transmitter locations
M=1; % number of transmitters
Tx=10^3*[-7]; % x-coords
Ty=10^3*[0]; % y-coords

% transmitter locations monostatic case
%M=N; % number of transmitters
%Tx=Rx; % x-coords
%Ty=Ry; % y-coords

% point targets
```

```
NN=1; % one target
XX=10^3*[0]; % x-coords
YY=10^3*[0]; % y-coords

% waveform employed (all transmitters use same waveform)
w=zeros(1,11);
w(4:8)=1; % step
%W=fftshift(fft(w)); % sinc function

%%%%%%%%% make appropriate data %%%%%%%%%%%%%
% Define Variables
c=3*10^8;               % Speed of Light
k_y=2*pi*(10^10)/c;     % wave vector @f=10 GHz
%k_y=1;
T=2e-3; % Total Data length in sec

delta_T=T/100; % Data resolution
D=zeros(N,1000); % large enough to absorb overlap of W and
the target scene size

for n=1:N % number of receivers (currently, set up as
monostatic)
for nn=1:NN % number of targets
R1=sqrt((Tx(1)-XX(nn))^2+(Ty(1)-YY(nn))^2);
R2=sqrt((Rx(n)-XX(nn))^2+(Ry(n)-YY(nn))^2);
tau=(R1+R2)/c;
m=ceil(tau/delta_T);
D(n,m+1:m+11)=D(n,m+1:m+11)+w; % superposition principle
end
end

save sample_data.mat Rx Ry Tx Ty w k_y T delta_T D N

imagesc(abs(D))
% read with: load "sample_data.mat" Rx Ry Tx Ty W k_y T
delta_T D
```

PREDICTED DATA MODEL CODE

```
%%%%%%%%%%%%%%%%%%%%%%%%%%%%%%%%%%%%%%%%%%%%%%%%%%%%%%%%%%%%%%%%%%%%%%%%
%% This Program creates the subrountine for the radar
model.
%%%%%%%%%%%%%%%%%%%%%%%%%%%%%%%%%%%%%%%%%%%%%%%%%%%%%%%%%%%%%%%%%%%%%%%%

%%
function d=predict(p,Rx,Ry,Tx,Ty,N,NN,w,k_y,T,delta_T)
```

```
c=3*10^8;
d=zeros(N,1000);

for n=1:N % number of receivers (currently, set up as
monostatic)
R1=sqrt((Tx(1)-p(1)).^2+(Ty(1)-p(2)).^2);
R2=sqrt((Rx(n)-p(1)).^2+(Ry(n)-p(2)).^2);
tau=mod((R1+R2)/c,1000);
m=ceil(tau/delta_T);
d(n,m+1:m+11)=d(n,m+1:m+11)+w;
end
```

POINT SPREAD FUNCTION CODE

```
%%%%%%%%%%%%%%%%
%  This program evaluates the Point Spread Function (PSF)
%  The program uses the approach, techniques on imaging from
Professor Borden, %  Brett

%  It is a six-parameter scattering model based on arbitrary
position
%  p=(p_x,p_y,p_z) & velocity u=(u_x,u_y,u_z)
%%%%%%%%%%%%%%%%

clear all

%%  Variables to be specified
x=(10^3)*[0;0;0];              % actual target
v=[0;0;0];                     % actual target velocity
y1=[2;0;0];                    % transmitter_1
z1=[-5;5;0];                   % receiver_1
z2=[15;15;0];                  % receiver_2
z3=[-2;-15;0];                 % receiver_3
z4=[-10;10;0];
z5=[0;14.1;0];
z6=[10;10;0];
z7=[14.1;0;0];
z8=[10;-10;0];
u=[0;0;0];
pulse=10^(-4);

%%  Parameters Defined
Y1=(1/sqrt(y1(1)^2+y1(2)^2+y1(3)^2)).*y1;
Z1=(1/sqrt(z1(1)^2+z1(2)^2+z1(3)^2)).*z1;
Z2=(1/sqrt(z2(1)^2+z2(2)^2+z2(3)^2)).*z2;
Z3=(1/sqrt(z3(1)^2+z3(2)^2+z3(3)^2)).*z3;
```

```
Z4=(1/sqrt(z4(1)^2+z4(2)^2+z4(3)^2)).*z4;
Z5=(1/sqrt(z5(1)^2+z5(2)^2+z5(3)^2)).*z5;
Z6=(1/sqrt(z6(1)^2+z6(2)^2+z6(3)^2)).*z6;
Z7=(1/sqrt(z7(1)^2+z7(2)^2+z7(3)^2)).*z7;
Z8=(1/sqrt(z8(1)^2+z8(2)^2+z8(3)^2)).*z8;
J=1;                            % Jacobian
c=3*10^8;
k_y=2*pi*(10^10)/c;             % wave vector @f=10 GHz

%%  PSF Range Defined
p_x_start=-20;
p_x_end=20;
p_y_start=-20;
p_y_end=20;
res_p=0.1;                      % resolution of p
p_x=p_x_start:res_p:p_x_end;  % define vector of x-axis
values
p_y=p_y_start:res_p:p_y_end;  % define vector of y-axis
values

%%  PSF Velocity Defined
u_x_start=-200;
u_x_end=200;
u_y_start=-150;
u_y_end=150;
res_u=1;
u_x=u_x_start:res_u:u_x_end;
u_y=u_y_start:res_u:u_y_end;

%%%%%%%%%%%%%%%%%
Localization in Position-Space
%%%%%%%%%%%%%%%%%

nx=length(p_x);                 % length of x = columns in K
ny=length(p_y);                 % length of y = rows in K
K=zeros(ny,nx);                 % initialize K matrix
K1=zeros(ny,nx);
K2=zeros(ny,nx);
K3=zeros(nx,ny);
K4=zeros(nx,ny);
K5=zeros(nx,ny);
K6=zeros(nx,ny);
K7=zeros(nx,ny);
K8=zeros(nx,ny);

for m=1:ny
    for n=1:nx
        p=(10^3)*[p_x_start+((n-1)*res_p);p_y_end-((m-
1)*res_p);0];

       % for receiver_1
       arg1_1=((Y1+Z1).')*((u*((Z1.')*p))-(v*((Z1.')*x)));
```

```
        phase1_1=exp(-i*k_y*arg1_1/c);
        arg2_1=((Y1+Z1).')*((p-x)+(0.5*(u-
v)*(((Y1+Z1).')*(p+x))));
        phase2_1=exp(i*k_y*arg2_1/c);
        tau_1=1/c*(((Y1+Z1).')*(p-x));
        neu_1=k_y*(((Y1+Z1).')*(u-v));
       %rectangular pulse
        amb_1=pi*(pulse-abs(tau_1))*exp(-
i*0.5*neu_1*pulse)*sinc((0.5/pi)*(-neu_1)*(pulse-
abs(tau_1)));
       K1(m,n)=phase1_1*phase2_1*amb_1*J;

       % for receiver_2
        arg1_2=((Y1+Z2).')*((u*((Z2.')*p))-(v*((Z2.')*x)));
        phase1_2=exp(-i*k_y*arg1_2/c);
        arg2_2=((Y1+Z1).')*((p-x)+(0.5*(u-
v)*(((Y1+Z2).')*(p+x))));
        phase2_2=exp(i*k_y*arg2_2/c);
        tau_2=1/c*(((Y1+Z2).')*(p-x));
        neu_2=k_y*(((Y1+Z2).')*(u-v));
        amb_2=pi*(pulse-abs(tau_2))*exp(-
i*0.5*neu_2*pulse)*sinc((0.5/pi)*(-neu_2)*(pulse-
abs(tau_2)));
        K2(m,n)=phase1_2*phase2_2*amb_2*J;

       % for receiver_3
        arg1_3=((Y1+Z3).')*((u*((Z3.')*p))-(v*((Z3.')*x)));
        phase1_3=exp(-i*k_y*arg1_3/c);
        arg2_3=((Y1+Z3).')*((p-x)+(0.5*(u-
v)*(((Y1+Z3).')*(p+x))));
        phase2_3=exp(i*k_y*arg2_3/c);
        tau_3=1/c*(((Y1+Z3).')*(p-x));
        neu_3=k_y*(((Y1+Z3).')*(u-v));
        amb_3=pi*(pulse-abs(tau_3))*exp(-
i*0.5*neu_3*pulse)*sinc((0.5/pi)*(-neu_3)*(pulse-
abs(tau_3)));
        K3(m,n)=phase1_3*phase2_3*amb_3*J;
        % for receiver_4
        arg1_4=((Y1+Z4).')*((u*((Z4.')*p))-(v*((Z4.')*x)));
        phase1_4=exp(-i*k_y*arg1_4/c);
        arg2_4=((Y1+Z4).')*((p-x)+(0.5*(u-
v)*(((Y1+Z4).')*(p+x))));
        phase2_4=exp(i*k_y*arg2_4/c);
        tau_4=1/c*(((Y1+Z4).')*(p-x));
        neu_4=k_y*(((Y1+Z4).')*(u-v));
        amb_4=pi*(pulse-abs(tau_4))*exp(-
i*0.5*neu_4*pulse)*sinc((0.5/pi)*(-neu_4)*(pulse-
abs(tau_4)));
        K4(m,n)=phase1_4*phase2_4*amb_4*J;

       % for receiver_5
        arg1_5=((Y1+Z5).')*((u*((Z5.')*p))-(v*((Z5.')*x)));
```

```
        phase1_5=exp(-i*k_y*arg1_5/c);
        arg2_5=((Y1+Z5).')*((p-x)+(0.5*(u-
v)*(((Y1+Z5).')*(p+x))));
        phase2_5=exp(i*k_y*arg2_5/c);
        tau_5=1/c*(((Y1+Z5).')*(p-x));
        neu_5=k_y*(((Y1+Z5).')*(u-v));
        amb_5=pi*(pulse-abs(tau_5))*exp(-
i*0.5*neu_5*pulse)*sinc((0.5/pi)*(-neu_5)*(pulse-
abs(tau_5)));
        K5(m,n)=phase1_5*phase2_5*amb_5*J;

       % for receiver_6
        arg1_6=((Y1+Z6).')*((u*((Z6.')*p))-(v*((Z6.')*x)));
        phase1_6=exp(-i*k_y*arg1_6/c);
        arg2_6=((Y1+Z6).')*((p-x)+(0.5*(u-
v)*(((Y1+Z6).')*(p+x))));
        phase2_6=exp(i*k_y*arg2_6/c);
        tau_6=1/c*(((Y1+Z6).')*(p-x));
        neu_6=k_y*(((Y1+Z6).')*(u-v));
        amb_6=pi*(pulse-abs(tau_6))*exp(-
i*0.5*neu_6*pulse)*sinc((0.5/pi)*(-neu_6)*(pulse-
abs(tau_6)));
        K6(m,n)=phase1_6*phase2_6*amb_6*J;

       % for receiver_7
        arg1_7=((Y1+Z7).')*((u*((Z7.')*p))-(v*((Z7.')*x)));
        phase1_7=exp(-i*k_y*arg1_7/c);
        arg2_7=((Y1+Z7).')*((p-x)+(0.5*(u-
v)*(((Y1+Z7).')*(p+x))));
        phase2_7=exp(i*k_y*arg2_7/c);
        tau_7=1/c*(((Y1+Z7).')*(p-x));
        neu_7=k_y*(((Y1+Z7).')*(u-v));
        amb_7=pi*(pulse-abs(tau_7))*exp(-
i*0.5*neu_7*pulse)*sinc((0.5/pi)*(-neu_7)*(pulse-
abs(tau_7)));
        K7(m,n)=phase1_7*phase2_7*amb_7*J;

       % for receiver_8
        arg1_8=((Y1+Z8).')*((u*((Z8.')*p))-(v*((Z8.')*x)));
        phase1_8=exp(-i*k_y*arg1_8/c);
        arg2_8=((Y1+Z8).')*((p-x)+(0.5*(u-
v)*(((Y1+Z8).')*(p+x))));
        phase2_8=exp(i*k_y*arg2_8/c);
        tau_8=1/c*(((Y1+Z8).')*(p-x));
        neu_8=k_y*(((Y1+Z8).')*(u-v));
        amb_8=pi*(pulse-abs(tau_8))*exp(-
i*0.5*neu_8*pulse)*sinc((0.5/pi)*(-neu_8)*(pulse-
abs(tau_8)));
        K8(m,n)=phase1_8*phase2_8*amb_8*J;

K(m,n)=(abs(K1(m,n)+K2(m,n)+K3(m,n)+K4(m,n)+K5(m,n)+K6(m,n)+
K7(m,n)+K8(m,n))).^2;
```

```
    end
end

%%%%%%%%%%%%%%%%
Localization in Velocity-Space
%%%%%%%%%%%%%%%%

nx=length(u_x);                % length of x = columns in K
ny=length(u_y);                % length of y = rows in K
K=zeros(ny,nx);
K1=zeros(ny,nx);
K2=zeros(ny,nx);
K3=zeros(ny,nx);
K4=zeros(ny,nx);
K5=zeros(ny,nx);
K6=zeros(ny,nx);
K7=zeros(ny,nx);
K8=zeros(ny,nx);

for m=1:ny
    for n=1:nx
        u=[u_x_start+((n-1)*res_u);u_y_end-((m-1)*res_u);0];

       % for receiver_1
        arg1_1=((Y1+Z1).')*((u*((Z1.')*p))-(v*((Z1.')*x)));
        phase1_1=exp(-i*k_y*arg1_1/c);
        arg2_1=((Y1+Z1).')*((p-x)+(0.5*(u-
v)*(((Y1+Z1).')*(p+x))));
        phase2_1=exp(i*k_y*arg2_1/c);
        tau_1=1/c*(((Y1+Z1).')*(p-x));
        neu_1=k_y*(((Y1+Z1).')*(u-v));
        amb_1=pi*(pulse-abs(tau_1))*exp(-
i*0.5*neu_1*pulse)*sinc((0.5/pi)*(-neu_1)*(pulse-
abs(tau_1)));
        K1(m,n)=phase1_1*phase2_1*amb_1*J;

       % for receiver_2
        arg1_2=((Y1+Z2).')*((u*((Z2.')*p))-(v*((Z2.')*x)));
        phase1_2=exp(-i*k_y*arg1_2/c);
        arg2_2=((Y1+Z1).')*((p-x)+(0.5*(u-
v)*(((Y1+Z2).')*(p+x))));
        phase2_2=exp(i*k_y*arg2_2/c);
        tau_2=1/c*(((Y1+Z2).')*(p-x));
        neu_2=k_y*(((Y1+Z2).')*(u-v));
        amb_2=pi*(pulse-abs(tau_2))*exp(-
i*0.5*neu_2*pulse)*sinc((0.5/pi)*(-neu_2)*(pulse-
abs(tau_2)));
        K2(m,n)=phase1_2*phase2_2*amb_2*J;

       % for receiver_3
        arg1_3=((Y1+Z3).')*((u*((Z3.')*p))-(v*((Z3.')*x)));
```

```
        phase1_3=exp(-i*k_y*arg1_3/c);
        arg2_3=((Y1+Z3).')*((p-x)+(0.5*(u-
v)*(((Y1+Z3).')*(p+x))));
        phase2_3=exp(i*k_y*arg2_3/c);
        tau_3=1/c*(((Y1+Z3).')*(p-x));
        neu_3=k_y*(((Y1+Z3).')*(u-v));
        amb_3=pi*(pulse-abs(tau_3))*exp(-
i*0.5*neu_3*pulse)*sinc((0.5/pi)*(-neu_3)*(pulse-
abs(tau_3)));
        K3(m,n)=phase1_3*phase2_3*amb_3*J;

       % for receiver_4
        arg1_4=((Y1+Z4).')*((u*((Z4.')*p))-(v*((Z4.')*x)));
        phase1_4=exp(-i*k_y*arg1_4/c);
        arg2_4=((Y1+Z4).')*((p-x)+(0.5*(u-
v)*(((Y1+Z4).')*(p+x))));
        phase2_4=exp(i*k_y*arg2_4/c);
        tau_4=1/c*(((Y1+Z4).')*(p-x));
        neu_4=k_y*(((Y1+Z4).')*(u-v));
        amb_4=pi*(pulse-abs(tau_4))*exp(-
i*0.5*neu_4*pulse)*sinc((0.5/pi)*(-neu_4)*(pulse-
abs(tau_4)));
        K4(m,n)=phase1_4*phase2_4*amb_4*J;

       % for receiver_5
        arg1_5=((Y1+Z5).')*((u*((Z5.')*p))-(v*((Z5.')*x)));
        phase1_5=exp(-i*k_y*arg1_5/c);
        arg2_5=((Y1+Z5).')*((p-x)+(0.5*(u-
v)*(((Y1+Z5).')*(p+x))));
        phase2_5=exp(i*k_y*arg2_5/c);
        tau_5=1/c*(((Y1+Z5).')*(p-x));
        neu_5=k_y*(((Y1+Z5).')*(u-v));
        amb_5=pi*(pulse-abs(tau_5))*exp(-
i*0.5*neu_5*pulse)*sinc((0.5/pi)*(-neu_5)*(pulse-
abs(tau_5)));
        K5(m,n)=phase1_5*phase2_5*amb_5*J;

       % for receiver_6
        arg1_6=((Y1+Z6).')*((u*((Z6.')*p))-(v*((Z6.')*x)));
        phase1_6=exp(-i*k_y*arg1_6/c);
        arg2_6=((Y1+Z6).')*((p-x)+(0.5*(u-
v)*(((Y1+Z6).')*(p+x))));
        phase2_6=exp(i*k_y*arg2_6/c);
        tau_6=1/c*(((Y1+Z6).')*(p-x));
        neu_6=k_y*(((Y1+Z6).')*(u-v));
        amb_6=pi*(pulse-abs(tau_6))*exp(-
i*0.5*neu_6*pulse)*sinc((0.5/pi)*(-neu_6)*(pulse-
abs(tau_6)));
        K6(m,n)=phase1_6*phase2_6*amb_6*J;

       % for receiver_7
        arg1_7=((Y1+Z7).')*((u*((Z7.')*p))-(v*((Z7.')*x)));
```

```
        phase1_7=exp(-i*k_y*arg1_7/c);
        arg2_7=((Y1+Z7).')*((p-x)+(0.5*(u-
v)*(((Y1+Z7).')*(p+x))));
        phase2_7=exp(i*k_y*arg2_7/c);
        tau_7=1/c*(((Y1+Z7).')*(p-x));
        neu_7=k_y*(((Y1+Z7).')*(u-v));
        amb_7=pi*(pulse-abs(tau_7))*exp(-
i*0.5*neu_7*pulse)*sinc((0.5/pi)*(-neu_7)*(pulse-
abs(tau_7)));
        K7(m,n)=phase1_7*phase2_7*amb_7*J;

       % for receiver_8
        arg1_8=((Y1+Z8).')*((u*((Z8.')*p))-(v*((Z8.')*x)));
        phase1_8=exp(-i*k_y*arg1_8/c);
        arg2_8=((Y1+Z8).')*((p-x)+(0.5*(u-
v)*(((Y1+Z8).')*(p+x))));
        phase2_8=exp(i*k_y*arg2_8/c);
        tau_8=1/c*(((Y1+Z8).')*(p-x));
        neu_8=k_y*(((Y1+Z8).')*(u-v));
        amb_8=pi*(pulse-abs(tau_8))*exp(-
i*0.5*neu_8*pulse)*sinc((0.5/pi)*(-neu_8)*(pulse-
abs(tau_8)));
        K8(m,n)=phase1_8*phase2_8*amb_8*J;

K(m,n)=(abs(K1(m,n)+K2(m,n)+K3(m,n)+K4(m,n)+K5(m,n)+K6(m,n)+
K7(m,n)+K8(m,n))).^2;

    end
end

%%%%%%%%%%%%%%%%
3-D Slice Plot for Position-Space
%%%%%%%%%%%%%%%%

p_x_start=-20;
p_x_end=20;
p_y_start=-20;
p_y_end=20;
p_z_start=-20;
p_z_end=20;
res_p=0.5;
p_x=p_x_start:res_p:p_x_end;   % define vector of x-axis
values
p_y=p_y_start:res_p:p_y_end;   % define vector of y-axis
values
p_z=p_z_start:res_p:p_z_end;

nx=length(p_x);                % length of x = columns in K
ny=length(p_y);                % length of y = rows in K
nz=length(p_z);                % length of z = pages in K
K=zeros(ny,nx,nz);             % initialize K matrix
K1=zeros(ny,nx,nz);
```

```
K2=zeros(ny,nx,nz);

for a=1:nz
    for m=1:ny
        for n=1:nx

            p=(10^3)*[p_x_start+((n-1)*res_p);p_y_end-((m-
1)*res_p);p_z_start+((a-1)*res_p)];

          % for receiver_1
            arg1_1=((Y1+Z1).')*((u*((Z1.')*p))-
(v*((Z1.')*x)));
            phase1_1=exp(-i*k_y*arg1_1/c);
            arg2_1=((Y1+Z1).')*((p-x)+(0.5*(u-
v)*(((Y1+Z1).')*(p+x))));
            phase2_1=exp(i*k_y*arg2_1/c);
            tau_1=1/c*(((Y1+Z1).')*(p-x));
            neu_1=k_y*(((Y1+Z1).')*(u-v));
            amb_1=pi*(pulse-abs(tau_1))*exp(-
i*0.5*neu_1*pulse)*sinc((0.5/pi)*(-neu_1)*(pulse-
abs(tau_1)));
            K1(m,n,a)=phase1_1*phase2_1*amb_1*J;

          % for receiver_2
            arg1_2=((Y1+Z2).')*((u*((Z2.')*p))-
(v*((Z2.')*x)));
            phase1_2=exp(-i*k_y*arg1_2/c);
            arg2_2=((Y1+Z1).')*((p-x)+(0.5*(u-
v)*(((Y1+Z2).')*(p+x))));
            phase2_2=exp(i*k_y*arg2_2/c);
            tau_2=1/c*(((Y1+Z2).')*(p-x));
            neu_2=k_y*(((Y1+Z2).')*(u-v));
            amb_2=pi*(pulse-abs(tau_2))*exp(-
i*0.5*neu_2*pulse)*sinc((0.5/pi)*(-neu_2)*(pulse-
abs(tau_2)));
            K2(m,n,a)=phase1_2*phase2_2*amb_2*J;

            K(m,n,a)=(abs(K1(m,n,a)+K2(m,n,a))).^2;

        end
    end
end

%%%%%%%%%%%%%%%%
Ambiguity Implementation for Chirp Signal
%%%%%%%%%%%%%%%%

        amb_1=pi*(pulse-abs(tau_1))*exp(i*0.5*(-
neu_1+(gamma*tau_1))*pulse)*sinc((0.5/pi)*(-
neu_1+(gamma*tau_1))*(pulse-abs(tau_1)));

%%%%%%%%%%%%%%%%
```

```
Output Plot
%%%%%%%%%%%%%%%%

clear all
image(p_x,p_y,64*K/max(max(K)))
hold on
plot(2,0,'+k',-5,5,'^k',15,15,'^k',-2,-15,'^k',15,-
15,'^k','linewidth',2)
hold off
xlabel({'\fontsize{11} x-component','\fontsize{11}
(position)'})
ylabel({'\fontsize{11} y-component','\fontsize{11}
(position)'})
title({'\fontsize{12} Transmitter/Receiver Geometry 1'})

% Slice Plot
norm=max(max(max(K)));
[UX,UY,UZ]=meshgrid(u_x,u_y,u_z);
slice(UX,UY,UZ,K/norm,[0],[0],[0])
colorbar
```

LIST OF REFERENCES

[1] B. Borden, *Radar imaging of airborne targets: A primer for applied Mathematicians and Physicists*, Taylor & Francis, 1999.

[2] M. Cheney and B. Borden, "Imaging moving targets from scattered waves," Institute of Physics Publishing on Inverse Problems, Vol. 24, April 2008.

[3] MAJ Tan Lu Pin, "Analysis of point spread function for imaging moving targets from scattered waves," Master's thesis, Physics Department, Naval Postgraduate School, December 2008.

[4] K. Tomiyasu, "Tutorial review of synthetic aperture radar (SAR) with applications to imaging of the ocean surface," Proceedings of the IEEE, Vol. 66, No. 5, pp. 563-583, May 1978.

[5] M. J. Gerry, L. C. Potter, I. J. Gupta and Andria van der Merwe, "A parametric model for synthetic aperture radar measurements," IEEE Trans Antennas and Propagation, Vol. 47, No. 7, pp. 1179-1188, July 1999.

[6] E. G. Larsson, G. Liu, P. Stocia and J. Li, "High-resolution SAR imaging with angular diversity," IEEE Trans Aerospace and Electronic Systems, Vol. 37, No. 4, pp. 1359-1372, October 2001.

[7] B. Borden and M. Cheney, "Synthetic aperture imaging from high-Doppler resolution measurements," Institute of Physics Publishing on Inverse Problems, Vol. 21, 2005.

[8] F. Berizzi, E. Dalle Mese, M. Diani and M. Martorella, "High-resolution ISAR imaging of maneuvering targets by means of the range instantaneous Doppler technique: Modeling and performance analysis," IEEE Trans Image Processing, Vol. 10, No. 12, pp. 1880-1890, December 2001.

[9] B. Zheng *et al*, "Time-frequency approaches to ISAR imaging of maneuvering targets and their limitations," IEEE Correspondence, 2001.

[10] T. Tsao, M. Slamani, P. Varshney, D. Weiner and H. Schwarzlander, "Ambiguity function for bistatic radar," IEEE Correspondence, 1997.

[11] B. Friedlander and B. Porat, "VSAR: A high resolution radar system for detection of moving targets," IEE Proc Radar, Sonar Navig., Vol. 144, No. 4, pp. 205-218, August 1997.

[12] Y. L. Wang et al., “Space-time adaptive processing for airborne radar with various array orientations,” IEE Proc Radar, Sonar Navig., Vol. 144, No. 6, pp. 330-340, December 1997.

[13] B. Borden, “Mathematical problems in radar inverse scattering,” Institute of Physics Publishing on Inverse Problems, Vol. 18, No. 1, February 2002.

[14] J. B. Keller, “Inverse problems,” The American Mathematical Monthly, Vol. 83, No. 2, pp. 107-118, February 1976.

[15] M. I. Skolnik, *Introduction to radar systems*, 2nd edition, McGraw-Hill, 2001.

[16] H. D. Griffiths, “Developments in modern synthetic aperture radar,” IEEE Radar Conference, pp. 734-739, April 2007.

[17] Ausherman et al., “Developments in radar imaging,” IEEE Trans Aerospace and Electronic Systems, Vol. AES-20, No. 4, pp. 363-400, July 1984.

[18] J. P. Zwart, *Aircraft recognition from features extracted from measured and simulated radar range profiles*, ASCI, The Netherlands, 2003.

[19] M. Cheney and B. Borden, *Fundamentals of radar imaging*, SIAM, 2009.

[20] “Radar,” class notes for PH 4274, Physics Department, Naval Postgraduate School, May 2008.

[21] V. C. Chen, H. Ling, “Time-Frequency Transforms for radar imaging and signal analysis,” *Norwood, MA: Artech House*, 2002.

[22] S. S. Jae, G. Thomas, B. C. Flores, “Range-Doppler radar imaging and motion compensation,” *Norwood, MA: Artech House*, 2001.

[23] M. Bertero and P. Boccacci, *Introduction to inverse problems in imaging*, pp. 81-86. Institute of Physics Publishing, UK, 1998.

[24] J. R. Guerci, *Space-time adaptive processing for radar*, Artech House, 2003.

[25] J. S. Bergin and P. M. Techau, “Multiresolution signal processing techniques for ground moving target detection using radar,” EURASIP Journal on Applied Signal Processing, No. 47534, 2006.

[26] G. Y. Wang *et al.*, “Dual-speed SAR imaging of moving targets,” IEEE Trans Aerospace and Electronic Systems, Vol. 42, No. 1, pp. 368-379, January 2006.

[27] J. K. Jao, “Theory of synthetic aperture radar imaging of a moving target,” IEEE Trans GeoScience and Remote Sensing, Vol. 39, No. 9, pp. 1984-1992, September 2001.

THIS PAGE INTENTIONALLY LEFT BLANK

INITIAL DISTRIBUTION LIST

1. Defense Technical Information Center
   Ft. Belvoir, Virginia

2. Dudley Knox Library
   Naval Postgraduate School
   Monterey, California

3. Professor James H. Luscombe
   Code PH/Lj
   Naval Postgraduate School
   Monterey, California

4. Professor Brett Borden
   Code PH/Bb
   Naval Postgraduate School
   Monterey, California

5. Professor Donald L. Walters
   Code PH/We
   Naval Postgraduate School
   Monterey, California

6. Teo Beng Koon William
   Ministry of Defence
   Singapore